

Pernille Moe Sagli

Infiltration based systems for stormwater management with multipurpose use

Master's thesis in Civil and Environmental Engineering

Supervisor: Tone Merete Muthanna

June 2020

Pernille Moe Sagli

Infiltration based systems for stormwater management with multipurpose use

Master's thesis in Civil and Environmental Engineering
Supervisor: Tone Merete Muthanna
June 2020

Norwegian University of Science and Technology
Faculty of Engineering
Department of Civil and Environmental Engineering

Project Description – spring 2020

Water and Wastewater Engineering

Title	Infiltration based systems for stormwater management with multipurpose use
Advisor	Tone Merete Muthanna
Place	Trondheim

The combined effects of climate change and urbanization are becoming increasingly evident in Norwegian cities, and subsequent increased stormwater runoff is a challenge. This has created a growing interest in well-functioning solutions for sustainable stormwater management. Deficient capacity in existing water infrastructure has led to a need for stormwater controls that contribute to reducing the load on piped systems. Multipurpose use systems for stormwater management are growing in popularity across the world. The functionality over time for such systems is of interest to municipalities and consultants; information may be useful input in decision-making and planning of future projects. Certain infiltration-based solutions can potentially reduce detention-volume requirements, which is beneficial in monetary terms and in restoring pre-development hydrological conditions.

In cooperation with Klima 2050 and Trondheim municipality, this thesis will study a pilot project on stormwater management at the newly established Trondheim town square. The stormwater facility combines infiltration and detention and is intended to relieve the load on the pipeline network. The system is constructed so that the detention is activated only when the infiltration system has reached its maximum capacity. The objective of the pilot project is to demonstrate and document the functionality of the stormwater management system under actual operational and maintenance conditions. A system for continuous data collection has been installed on site, and the current study aims to assess the following thesis statement:

To what extent can infiltration capacity of a system be estimated through continuous online monitoring of hydrological aspects accompanied with current knowledge on local soil conditions?

Assessment of the thesis statement will be complemented with the following research questions:

1. What are the strengths and weaknesses of the established system at Trondheim town square with respect to infiltration monitoring?
2. What improvements can be made to the system to increase the usability for infiltration monitoring?
3. Preliminary analysis of system performance with respect to infiltration.

Collaboration partners: Klima 2050 and Trondheim kommune
Workplace: IBM

Abstract

Stormwater challenges as a result of climate change and continued urban development is a growing concern around the world. This has created an increasing need for sustainable stormwater management (SWM) solutions, and the interest in multipurpose use systems is growing. Infiltration based systems reduce the overall volume of stormwater runoff, but despite the growth in popularity their long-term functionality is uncertain.

This thesis studied a pilot project with the objective of finding the extent that infiltration capacity can be estimated through continuous online monitoring of various hydrological aspects accompanied with current knowledge on local soil conditions. The pilot, located on the newly upgraded Trondheim town square, combines infiltration and detention in a design aimed to reduce the load on the downstream piped network. Following data processing, a preliminary analysis of the data series was performed. The strengths and weaknesses of the established system with respect to infiltration monitoring were analysed and suggestions for future improvements discussed.

Thorough data analysis has shown that there are substantial inconsistencies. Even after processing, imperfections in the data series are apparent. Inaccurate input variables, thereby inflow and outflow, has resulted in uncertain infiltration calculations that periodically are substantially lower than expected. Inflow was measured using an area-velocity flow meter that was subject to noise and had an incorrect threshold for zero flow. Outflow was determined from calculations based on pressure head that were highly uncertain for low water levels. Installing a flow meter on the downstream end of the facility may better the quality of outflow data. Otherwise, data quality may be improved by ensuring sensors are correctly calibrated and shielded from external disturbances.

The absence of local precipitation data and the approximate drainage area are significant limitations to the study that made comparison to the measured data on site intricate. Thus, installing a rain gauge closer to the study site should be a priority in future work. Moreover, data show that the detention basins were rarely utilized and that even for moderately sized rainfalls the amount of stored water was small. However, since the divers used for water level monitoring were installed at a later stage of the study, basin performance during heavy rainfalls is still uncertain.

The study concludes that infiltration capacity can to some extent be estimated from measured data and soil properties, but not with great accuracy. It is therefore recommended that the suggested modifications of the monitoring system are implemented prior to continued research to ensure that high data quality is obtained. This may be a key element when verifying the proposed infiltration capacity of the stormwater facility and be useful in analysis of its long-term functionality.

Sammendrag

Overvannsproblematikk grunnet klimaendringer og stadig utvikling av urbane områder er en voksende utfordring rundt om i verden. Dette har ført til økende behov for bærekraftige løsninger for overvannshåndtering, og interessen for flerbrukssystemer er økende. Infiltrasjonsbaserte systemer reduserer det totale volumet av overvannsavrenning, men til tross for økt popularitet er langtidsfunksjonaliteten uvisst.

Denne masteroppgaven omhandler et pilotprosjekt med mål om å finne hvorvidt infiltrasjonskapasitet kan estimeres ved hjelp av kontinuerlig overvåkning av ulike hydrologiske aspekter kombinert med nåværende kunnskap om lokale grunnforhold. Piloten, som befinner seg på det nylig oppgraderte Torvet i Trondheim, kombinerer infiltrasjon og fordrøyning i et system designet for å avlaste det lukkede nedstrøms rørsystemet. Innsamlet måledata ble prosessert og senere analysert. Styrker og svakheter ved det etablerte målesystemet ble vurdert med hensyn til infiltrasjonsovervåkning og forslag til framtidige forbedringer ble diskutert.

Omfattende dataanalyse har vist vesentlige uoverensstemmelser. Selv etter prosessering er svakhetene ved dataseriene tydelige. Unøyaktige inndata, derav inn- og utstrømming, har ført til usikre infiltrasjonsberegninger som periodevis er vesentlig lavere enn forventet. Innstrømming ble målt med en støyutsatt areal-hastighetsbasert vannmåler hvor nivået for null strømming var feil. Utstrømming ble beregnet fra formelverk basert på trykkehøyde som var svært unøyaktig for lave vannivåer. Å montere en vannmåler på nedstrøms side av anlegget kan bedre kvaliteten av utstrømningsdata. Ellers kan datakvalitet forbedres ved å forsikre at måleinstrumentene er riktig kalibrert og skjermet fra ytre forstyrrelser.

Mangelen på lokal nedbørsdata og det omtrentlige tilrenningsarealet er to vesentlige svakheter ved studien som gjorde sammenlikning med annen måledata utfordrende. Derfor bør montasje av en nedbørsmåler nærmere anlegget prioriteres i framtidig arbeid. Måledata viser imidlertid at fordrøyningsbassengene sjelden ble utnyttet og at mengden lagret overvann var liten selv for større nedbørshendelser. Likevel er det uvisst hvordan fordrøyningsbassengene vil opptre ved store regnmengder, siden måleutstyret ble installert på et senere tidspunkt i studien.

Studien fastsetter at infiltrasjonskapasitet til en viss grad kan bli anslått basert på måledata og kjente grunnforhold, men uten stor nøyaktighet. Derfor anbefales det at de foreslåtte forbedringene av målesystemet implementeres i forkant av videre arbeid med piloten slik at bedre datakvalitet oppnås. Dette kan være et viktig element i bekreftelsen av den antatte infiltrasjonskapasiteten og være nyttig i analyser av systemets langtidsfunksjonalitet.

Preface

This Master thesis marks the completion of the course TVM4905 – Water Supply and Wastewater Systems and the civil and environmental engineering education at the Norwegian University of Science and Technology (NTNU). Infiltration based system for urban stormwater management was the topic of this Master thesis and my project thesis, titled “Effect of urbanization on soil infiltration properties and urban hydrology”, was a preliminary work done in the fall of 2019.

My greatest gratitude goes to my supervisor, Associate Professor Tone Merete Muthanna at NTNU for all guidance, support and encouragement through the writing process. I greatly appreciate everything you have done and for all the insightful comments and suggestions. A special thank you to Birgitte Gisvold Johannessen at Trondheim municipality for all advice, support, and assistance with field work and other practical matters.

Thank you also to the following people and organizations:

- Klima 2050 for the opportunity to write this thesis
- Trondheim bydrift for help with field work
- Brynjar Bremset at Multiconsult for clarifications on the system design
- Assistant Professor Arnfinn Emdal at NTNU for help with analysing rotary-pressure soundings
- Phd candidate at NTNU, Elhadi Mohsen Hassan Abdalla, for help with programming
- Nils Aaby at MFT for helpful suggestions on swirl chamber calculations

Lastly, my greatest thanks to my loving and supportive family and friends. I am endlessly grateful for all the help and encouragement you have given me throughout my years of study.

Trondheim, June 5th, 2020

Pernille Moe Sagli

Pernille Moe Sagli

Content

Figures	xii
Tables	xii
Equations	xiii
Abbreviations	xiii
1 Introduction	1
1.1 Background	1
1.2 Scope and research questions	3
2 Stormwater theory	4
2.1 Stormwater management.....	4
2.1.1 Stormwater detention	5
2.1.2 Three-step strategy	7
2.2 Low-impact development	8
3 Infiltration and percolation theory	9
3.1 Soil properties	9
3.1.1 Hydraulic conductivity.....	10
3.2 Formulas.....	12
3.3 Dimensioning of infiltration systems	14
3.4 Urbanization impacts	14
3.4.1 Urban karst	15
3.5 Climatic impacts.....	15
4 Description of pilot	17
4.1 Site description	17
4.1.1 Ground conditions	18
4.2 Stormwater facility	22
4.2.1 Design basis	24
5 Method	26
5.1 Data collection	26
5.2 Drainage area delineation.....	28
5.3 Calculation of infiltration and percolation	28
6 Data processing	29
6.1 Water levels	29
6.2 Inflow	29
6.2.1 Noise	29
6.2.2 Threshold level	30
6.3 Outflow.....	30

6.3.1	Outflow at low water levels.....	30
7	Results and discussion.....	34
7.1	Drainage area.....	34
7.2	Analysis of collected data.....	35
7.2.1	Precipitation.....	35
7.2.2	Inflow.....	35
7.2.3	Outflow.....	36
7.3	Analysis of rain events.....	36
7.4	Detention basin performance.....	44
7.5	Infiltration capacity evaluation.....	44
7.6	Possible system improvements.....	45
7.6.1	Inflow.....	45
7.6.2	Outflow.....	45
7.6.3	Precipitation.....	45
7.6.4	Infiltration and detention.....	45
8	Conclusion.....	47
8.1	Further work.....	48
	References.....	49
	Appendices.....	53

Figures

Figure 1.1: Temperature derogation from the normal in Trøndelag	1
Figure 1.2: Effect of urbanization on peak runoff rate.....	2
Figure 2.1: IDF-curve for Voll – Tyholt – Moholt in Trondheim.....	5
Figure 2.2: Detention volume and discharge for separate systems	6
Figure 2.3: Detention volume and discharge for combined systems	7
Figure 2.4: Hydrograph of pre-development condition (1), conventional stormwater controls (2), and LID (3)	8
Figure 3.1: Principle of downward water movement through soil	9
Figure 3.2: Infiltration capacity over duration of rainfall	12
Figure 3.3: Water retention curve for sand, loam, and clay	13
Figure 3.4: Urban karst principle	15
Figure 4.1: Geographical location of Trondheim.....	17
Figure 4.2: Satellite photo of Trondheim city centre.....	18
Figure 4.3: Location of drilling points	19
Figure 4.4: Rotary pressure sounding at point 1	21
Figure 4.5: Rotary pressure sounding at point 3	21
Figure 4.6: Rotary pressure sounding and soil sampling at point 2.....	22
Figure 4.7: Functioning of FluidVetric VSU swirl chamber.....	23
Figure 4.8: Flow chart of the infiltration and detention system	23
Figure 4.9: Inside of the detention basin looking north.....	25
Figure 5.1: CTD-diver installation	27
Figure 5.2: Baro-diver installation	27
Figure 6.1: Uncertainty of outflow from swirl chamber	31
Figure 6.2: Water level references in swirl chamber.....	32
Figure 6.3: Outflow response to different water levels.....	33
Figure 7.1: Drainage area from delineation	34
Figure 7.2: Results from Event 1	37
Figure 7.3: Results from Event 2	38
Figure 7.4: Results from Event 3	39
Figure 7.5: Results from Event 4	41
Figure 7.6: Results from Event 5	42
Figure 7.7: Results from Event 6	43

Tables

Table 3.1: Hydraulic conductivities of common soil types.....	11
Table 4.1: Geotechnical reports on Trondheim town square	18
Table 4.2: Results from Report 0200.....	20
Table 4.3: Results from Report 1129.....	20
Table 6.1: Differences in sensor and measured water levels.....	29
Table 7.1: Results from Event 1	36
Table 7.2: Results from Event 2	38
Table 7.3: Results from Event 3	39
Table 7.4: Results from Event 4	40
Table 7.5: Results from Event 5	42
Table 7.6: Results from Event 6	43

Equations

Equation (1): Rational method	4
Equation (2): Reduced area	6
Equation (3): Soil porosity	9
Equation (4): Volumetric water content	10
Equation (5): Soil saturation	10
Equation (6): Effective saturation	10
Equation (7): Hydraulic conductivity	11
Equation (8): Horton's equation	12
Equation (9): Van Genuchten equation	12
Equation (10): Darcy's law	13
Equation (11): Simplified Darcy's law	14
Equation (12): System infiltration capacity	14
Equation (13): Infiltration rate at timestep	28
Equation (14): Event water volume	28
Equation (15): Total head above swirl chamber centre line	30
Equation (16): Pressure loss over nozzle threshold of swirl chamber	32
Equation (17): Torricelli's law	32
Equation (18): Cross-sectional area of circular pipe	33

Abbreviations

DEM	Digital Elevation Model
DN	Nominal diameter
GIS	Geographic Information System
IDF	Intensity-Duration-Frequency
ITAS	Scanmatic Instrument Technology AS
K_{sat}	Saturated hydraulic conductivity
LID	Low-impact development
m.a.s.l.	Meters above sea level
MOUSE	Model for urban sewers
NTNU	Norwegian University of Science and Technology
PP	Polypropylene
SN	Nominal stiffness
SuDS	Sustainable urban drainage systems
SWM	Stormwater management
SWMM	Stormwater management model

1 Introduction

1.1 Background

The effects of climate change are becoming increasingly evident (Eckart, McPhee and Bolisetti, 2017) and in combination with urbanization and ecological concerns this calls for new stormwater management (SWM) strategies. Historical data show that the yearly precipitation in Trøndelag county has increased over the past century and is especially evident in the last 20 years, as can be seen in Figure 1.1 (Meteorologisk institutt, 2017). In future years, it is expected that high-intensity rain events will be more frequent with a corresponding increased risk of rainfall flooding (Norsk Klimaservicesenter, 2016).

Trøndelag has also gotten warmer over the past 100 years; since 1985, temperatures have been higher than normal with a tendency of continued warming (Norsk Klimaservicesenter, 2016). Model calculations show that by the end of the 21st century the yearly average temperature likely will rise by approximately 4.0°C while precipitation increases with 20%. The proposed climatic changes vary seasonally and spatially. The largest temperature increases are expected in the fall, winter and spring. Precipitation increase is expected to be largest for the summer and fall and most evident in the coastal regions of the county.

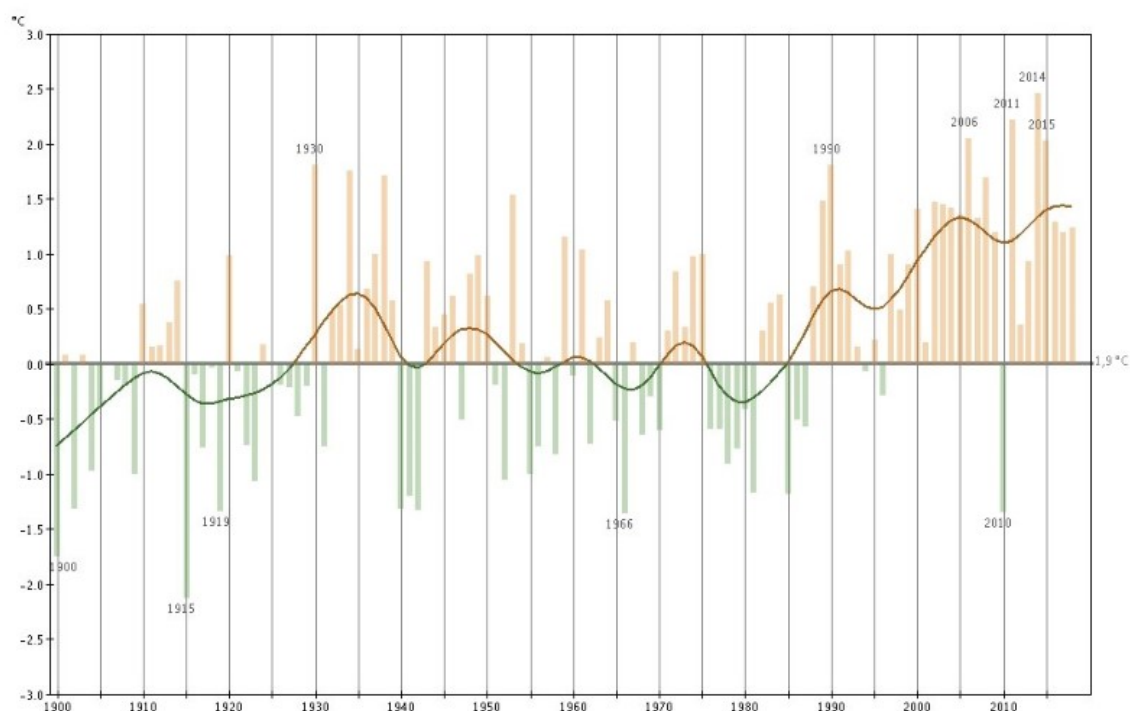


Figure 1.1: Temperature derogation from the normal in Trøndelag (Meteorologisk institutt, 2017).

In combination with climate change, excessive urbanization imposes water-related challenges (Eckart, McPhee and Bolisetti, 2017). Urbanization often involves changes that alter the natural hydrologic cycle, such as vegetation removal and the establishment of more impervious surfaces (Ødegaard *et al.*, 2014). Consequently, these effects can lead

to less evaporation and infiltration while surface runoff and erosion increases. Figure 1.2 illustrates the effect of urbanization on peak runoff rate.

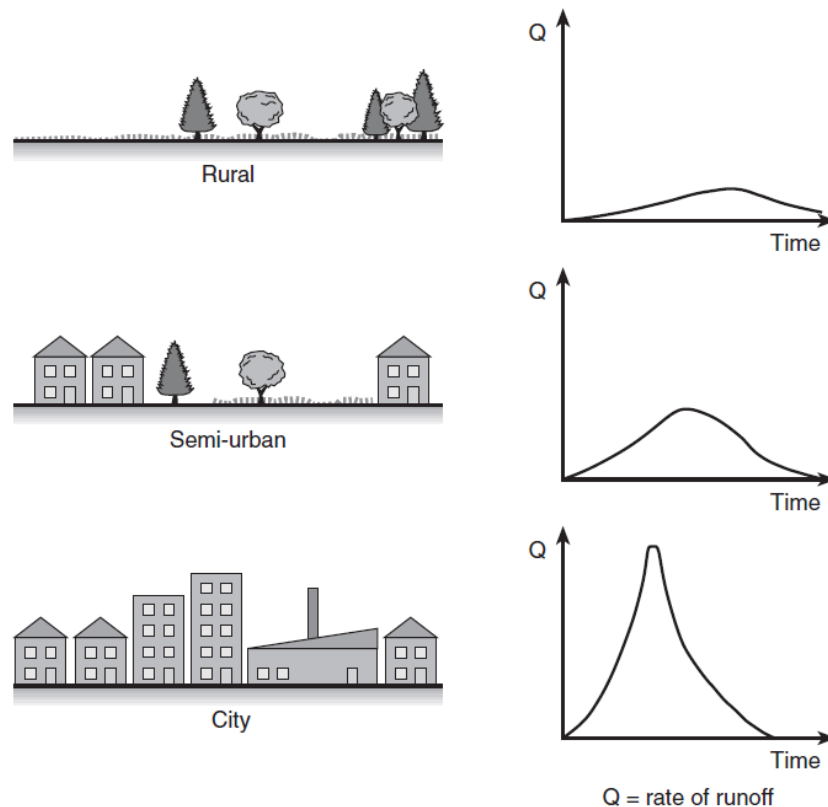


Figure 1.2: Effect of urbanization on peak runoff rate (Butler and Davies, 2011).

As populations grow, there is a continuous need for further urban development. The United Nations (2019b; 2019a) propose that the majority of further population growth will occur in urban areas. It is expected that the population in Trondheim will be 220 545 in 2040; this corresponds to an 11% increase in population compared to the 198 219 inhabitants in 2019 (Statistisk sentralbyrå, 2020c). Other major Norwegian cities, for example Oslo and Bergen, are also expected to experience substantial population growth (Statistisk sentralbyrå, 2020a; 2020b). Evidently, there is a need for urban development.

Several problems related to future SWM arise as a result of combined urbanization and climate change (Trondheim kommune, 2013). Existing piped sewer systems, both combined and separate, may experience capacity-related problems. More basement flooding occurrences, increased pollution, as well as surface flooding are possible consequences.

In recent years, Norwegian municipalities have been engaged in sustainable solutions for SWM as they continue to face challenges related to climate change. Several projects have been conducted on various solutions for sustainable SWM in cold climates, including green and grey roofs (Johannessen and Muthanna, 2018; Johannessen, Hanslin and Muthanna, 2017) and bioretention cells (Balstad *et al.*, 2018; Paus, Muthanna and Braskerud, 2016). Such research is valuable for future projects in Norway and other areas expected to meet future challenges related to SWM.

1.2 Scope and research questions

In cooperation with Klima 2050, Trondheim municipality has recently built a stormwater facility at the newly upgraded town square in the city centre. The system design combines stormwater infiltration with backup detention basins. In cooperation with the municipality, Klima 2050 is researching the pilot project with the aim of documenting and verifying the functionality of the infiltration system over time. Interest points include system capacity and the frequency of overflow activation to the detention basins. In the long term, these results may be used for evaluating the extent that infiltration systems can reduce detention volume requirements in urban areas and potentially for developing a system model for designing such systems in the future.

Various sensors have been installed at the facility for continuous monitoring of water levels and flow. Instrumentation was installed early on in 2020 and collected data has so far not been used in research. Thus, the quality of collected data and the monitoring system itself is uncertain. The current study aims to evaluate the usefulness of the established system with respect to infiltration monitoring. Thematically, this study is limited to the hydrological aspects of SWM and will not discuss pollution control in detail. Geographically, the study is limited to the Trondheim town square and the specific stormwater facility in question. Thus, the thesis statement to be assessed is the following:

To what extent can infiltration capacity be estimated through continuous online monitoring of hydrological aspects accompanied with current knowledge on local soil conditions?

Assessment of the thesis statement will be complemented with the following three research questions, that are aimed to be answered through evaluation of measured data:

1. What are the strengths and weaknesses of the established system at Trondheim town square with respect to infiltration monitoring?
2. What improvements can be made to the system to increase the usability for infiltration monitoring?
3. Preliminary analysis of system performance with respect to infiltration.

First, background theory from existing journal articles, books, and reports on stormwater, infiltration and percolation is presented. Then, a description of the study site and stormwater facility is presented. The study methodology is described followed by a separate description of data processing. Next, results are presented and discussed with respect to the presented theory and the research questions. To conclude the study, the most important findings are summarized, the research questions and the thesis statement are answered, and suggestions for further work are presented.

2 Stormwater theory

Stormwater is a collective term for water that flows on the ground surface, generated by precipitation and snowmelt (Ødegaard *et al.*, 2014; Skaaraas *et al.*, 2015). In the natural hydrologic cycle, much of this water is infiltrated to the subgrade soil and transported to watersheds, and some is transported back to the atmosphere through evapotranspiration. Urban development disturbs the natural hydrologic cycle and the hydrological processes it involves. A principal challenge is the change in ground cover from pervious to impervious surfaces which creates increased amounts of surface runoff.

If not handled adequately, stormwater has the potential to cause major structural damage and health risks. Urban areas are especially vulnerable to damages caused by stormwater that, according to Magnussen *et al.* (2015), result in significant expenditures. In report NOU 2015:16, yearly costs due to stormwater damages in Norway are estimated to 1.6 to 3.6 billion NOK (Skaaraas *et al.*, 2015). With the absence of preventative measures, these costs are expected to increase in correlation with future urbanization and climate change.

2.1 Stormwater management

SWM is essential in maintaining public health and safety (Butler and Davies, 2011), and is of high social, economical, and ecological importance. SWM refers to the activities and measures in place to utilize stormwater as a resource, while preventing damage and disadvantages caused by stormwater (Skaaraas *et al.*, 2015).

The basis for effective SWM is knowledge about the amount of generated stormwater in an area (Ødegaard *et al.*, 2014). Different methods for calculating stormwater amounts are used depending on the catchment size and how vulnerable the area is to damages caused by stormwater. In practice, Equation (1) known as the rational method is often used for urban catchments smaller than 50 ha.

$$Q = \varphi \cdot A \cdot I \cdot C \quad (1)$$

where

Q = runoff [l/s]
 φ = runoff coefficient [-]
 A = catchment area [ha]
 I = rain intensity [l/s·ha]
 C = climate factor [-]

The runoff coefficient is the ratio between surface runoff and precipitation (Ødegaard *et al.*, 2014). It depends on the type of surface; impervious surfaces, such as roofs and asphalt-covered roads and parking lots have a high runoff coefficient, while natural forest has a low value. Recommendations on runoff coefficients are provided by for example COWI (2015), but should be evaluated based on specific site characteristics. In cases with mixed areal use, a weighted average runoff coefficient may be used. Moreover, a runoff coefficient below 0.3 should be avoided in order to take consideration of winter conditions (Trondheim kommune, 2015).

The rain intensity is determined from local Intensity-Duration-Frequency (IDF) curves; rain intensities for different combinations of rain durations and return periods are given in a graph or table, such as Figure 2.1. Each colour represents a different return period given in years. The climate factor is included to account for future increases in precipitation. Trondheim municipality operates with a factor of 1.2, meaning future precipitation is expected to increase by 20% (Trondheim kommune, 2015). However, using a higher climate factor is more conservative, and Lindholm (2018) suggests using a factor of 1.4 for intense rainfalls. For catchments larger than 50 ha or catchments especially vulnerable to stormwater damages, computer-based hydraulic models, such as SWMM (Stormwater Management Model) and MOUSE (Model for Urban Sewers), should be used for calculating runoff (Ødegaard *et al.*, 2014).

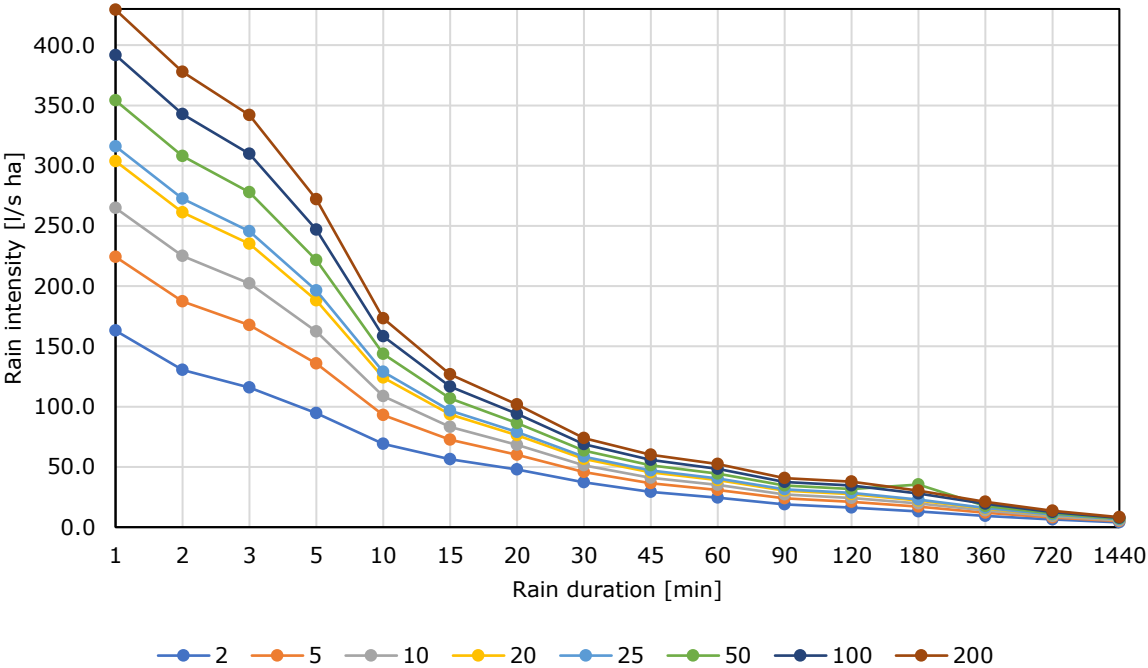


Figure 2.1: IDF-curve for Voll – Tyholt – Moholt in Trondheim. Figure adapted from Trondheim kommune (2015).

2.1.1 Stormwater detention

Stormwater detention refers to temporary storage of runoff (Water Environment Federation and ASCE, 2012). The intention of stormwater detention is to decrease peak flows generated by increased runoff volumes and thereby avoid exceeding the capacity of downstream pipes. Due to limited capacity in existing stormwater pipes, stormwater discharge regulations are usually needed; municipalities set restrictions on the amount of stormwater that can be released onto the piped network. Several detention alternatives exist, and underground technologies have traditionally been dominating. These include buried cassettes and large concrete or plastic pipes. A restricted outflow is achieved by using a regulator, for example a swirl chamber.

Dimensioning of detention basins

In Trondheim municipality, required detention volume is calculated graphically with reduced area as the input variable. Reduced area is calculated as follows (Trondheim kommune, 2015):

$$\text{Reduced area} = A \cdot \varphi \quad (2)$$

where

A = catchment area [ha]

φ = runoff coefficient [-]

Depending on whether the sewer system is separate or combined, the required detention and corresponding stormwater discharge are found from Figure 2.2 and Figure 2.3, respectively.

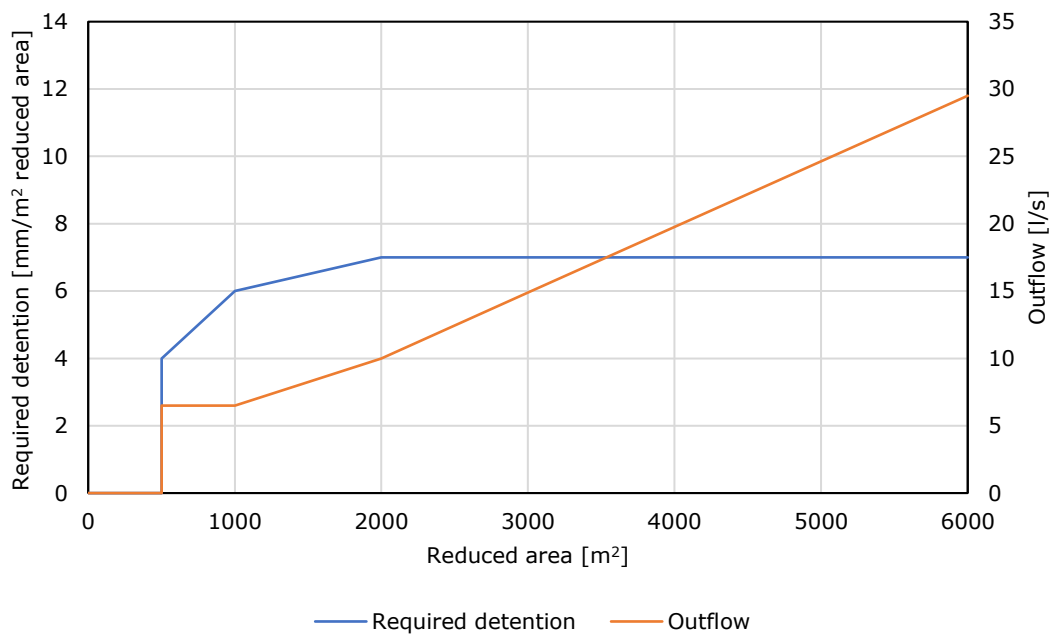


Figure 2.2: Detention volume and discharge for separate systems. Figure adapted from Trondheim kommune (2015).

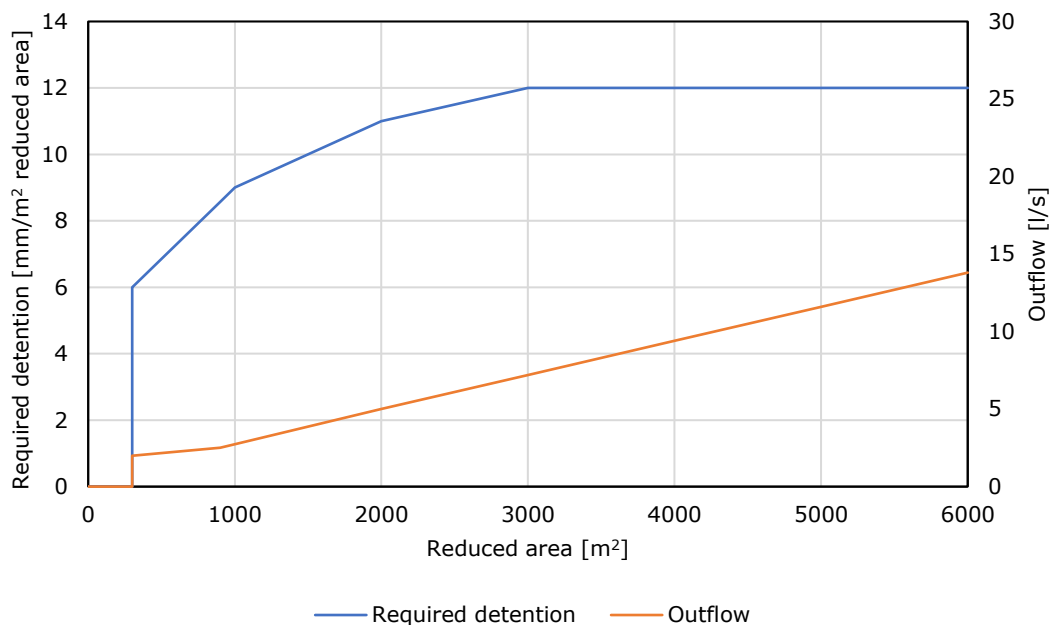


Figure 2.3: Detention volume and discharge for combined systems. Figure adapted from Trondheim kommune (2015).

Trondheim municipality uses a rainfall with a return period of 20 years and a safety factor of 1.2 when calculating required detention volume and discharge. In certain cases it is necessary to compare the graphically determined detention volume to the calculated detention volume from the "rain envelope method" based the mass balance of a box rain for various durations (Lindholm *et al.*, 2012).

2.1.2 Three-step strategy

Traditionally, SWM has focused on safe and rapid removal of surface runoff (Ødegaard *et al.*, 2014; Ballard *et al.*, 2015). This involves utilizing grey infrastructure that leads stormwater to a drain and transports it to the recipient through underground piping systems (Lindholm *et al.*, 2008). The traditional approach to SWM is still widely used, but Norwegian municipalities are becoming increasingly aware of its environmental and economic drawbacks.

Currently, it is emphasized that SWM is a multi-disciplinary task that should be integrated in the early planning phases of projects (Ødegaard *et al.*, 2014; Lindholm *et al.*, 2008; Ballard *et al.*, 2015). Coordinated SWM solutions with vegetation and road planning are feasible. Ponds, creeks and other surface water bodies are considered to be aesthetic and valuable implementations in landscaping if planned correctly. Moreover, caution should be taken, and careful consideration of capacity is essential to ensure communal safety. Lindholm *et al.* (2008) developed a three-step strategy for SWM in Norwegian municipalities:

1. Collect and infiltrate small rainfalls
2. Slow down and detain medium sized rainfalls
3. Establish safe waterways for large rainfalls

The guideline suggests that rainfalls below 20 mm are categorized as small, rainfalls between 20 and 40 mm as medium, and above 40 mm as large. However, the rain size within each category should be evaluated for each project. The first step in the three-step

strategy emphasises the use of blue-green infrastructure and SWM at the site-scale. This involves the establishment of low-impact development (LID) systems which will be explained in the following.

2.2 Low-impact development

LID, also known as sustainable urban drainage systems (SuDS), is a design philosophy that aims to mimic pre-development hydrological processes and conditions (University of Arkansas Community Design Center, 2010; Ballard *et al.*, 2015). As described, urbanization creates larger stormwater runoff volumes and subsequent higher peak flows. LID mitigate these effects through distributed on-site controls for local management of stormwater runoff. Figure 2.4 illustrates how hydrographs of conventional stormwater controls and LID compare to that of pre-development conditions.

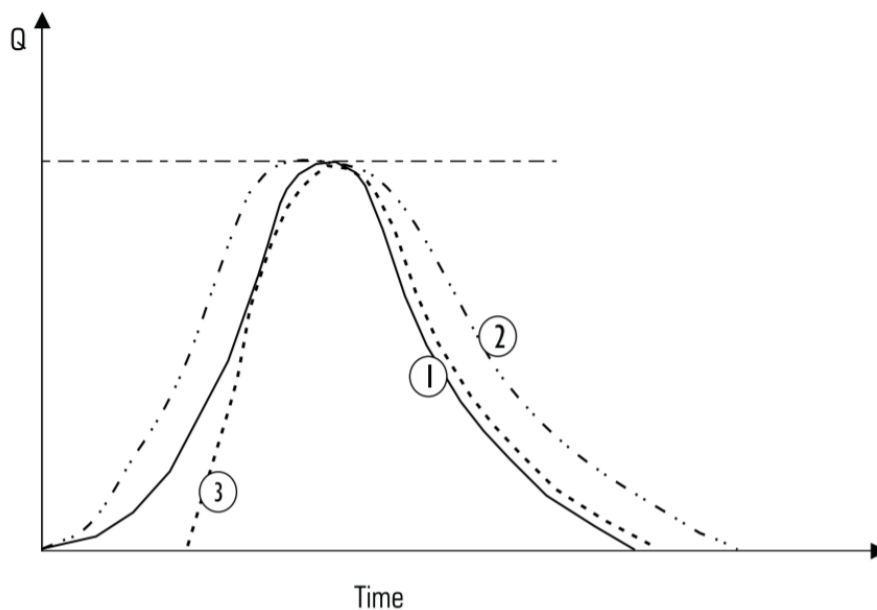


Figure 2.4: Hydrograph of pre-development condition (1), conventional stormwater controls (2), and LID (3) (Prince George's County, 1999).

LID is commonly classified as either retention-based or infiltration-based (Fletcher, Andrieu and Hamel, 2013). Retention-based controls temporarily detain stormwater and reduce outflow. Examples include ponds, green roofs, rainwater harvesting, and wetlands. Such solutions are helpful in reducing the load on downstream infrastructure, but do not reduce the total volume of stormwater to a great extent as their losses are due to evapotranspiration alone (Fletcher, Andrieu and Hamel, 2013).

Net runoff volume reduction is today considered necessary for sustainable SWM (Sage, Berthier and Gromaire, 2015). Infiltration-based LID controls retain stormwater (Fletcher, Andrieu and Hamel, 2013), and are considered effective in restoring pre-development hydrological conditions (Ballard *et al.*, 2015). Examples of technologies include bioretention cells or raingardens, pervious pavements, infiltration trenches and swales, and infiltration basins or soakaways (Eckart, McPhee and Bolisetti, 2017).

3 Infiltration and percolation theory

Infiltration and percolation both refer to the movement of water through porous materials, and although the terms are sometimes used interchangeably, the processes differ slightly. Infiltration is the process in which surface water enters the soil, whereas percolation is the downward flow in the unsaturated zone of subsurface soils (Dingman, 2015), as illustrated in Figure 3.1. These processes are closely linked and play an important role in the hydrologic response to rainfall or snowmelt. After surface water is infiltrated it can either be transported to surface waters through underground paths, be retained in the soil and ultimately re-enter the atmosphere through evapotranspiration, or eventually contribute to groundwater recharge.

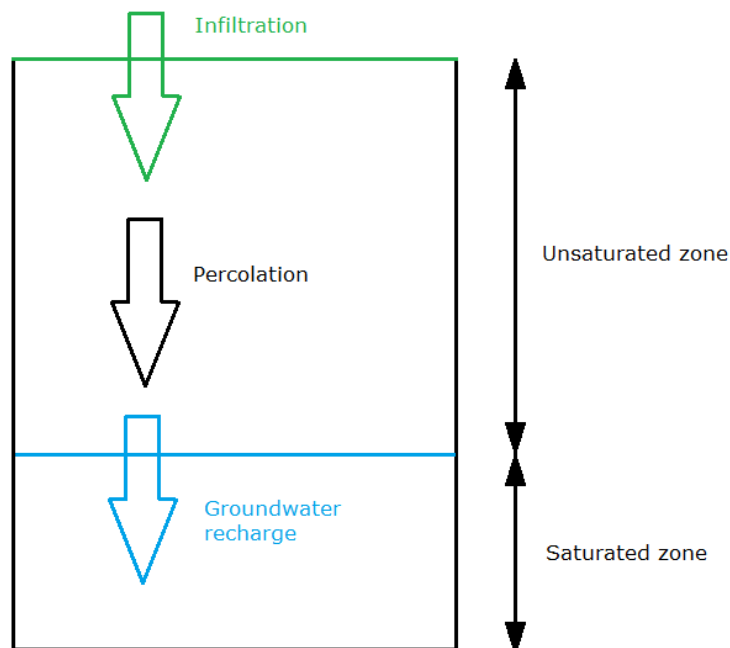


Figure 3.1: Principle of downward water movement through soil.

Infiltration capacity is commonly described as infiltration rate with a unit of distance over time (Butler and Davies, 2011). The amount of water that is infiltrated depends on the rainfall or snowmelt volume, site characteristics and soil properties.

3.1 Soil properties

Soil properties are decisive for infiltration and percolation. Soil is a porous medium which makes penetration and infiltration of water possible. Porosity and volumetric water content both play a role in flow characteristics. Porosity is the proportion of pore spaces in a soil volume and is calculated as follows (Dingman, 2015):

$$\phi = \frac{V_a + V_w}{V_s} \tag{3}$$

where

$$\begin{aligned}\phi &= \text{porosity [-]} \\ V_a &= \text{volume of air [m}^3\text{]} \\ V_w &= \text{volume of water [m}^3\text{]} \\ V_s &= \text{total soil volume [m}^3\text{]}\end{aligned}$$

Porosity is affected by grain size and shape, compaction, and grain-size distribution. For example, in a soil sample with large grain-size distribution, the smaller grains will likely fill the void spaces between the larger grains, making the soil less porous. Roughly shaped fine-grained soils, such as clay, may be arranged in an open structure that is maintained by electrostatic forces, and thereby still obtain a high porosity. Volumetric water content, or soil-moisture content, is the ratio of water volume to soil volume:

$$\theta = \frac{V_w}{V_s} \quad (4)$$

where

$$\begin{aligned}\theta &= \text{volumetric water content [-]} \\ V_w &= \text{volume of water [m}^3\text{]} \\ V_s &= \text{total soil volume [m}^3\text{]}\end{aligned}$$

The water content in soils is not constant spatially or in time and can in theory range from 0 to 100% for completely dry and saturated conditions, respectively. However, natural soils will usually contain some water held by surface tension and electrostatic forces. Thus, the lower limit will be greater than 0. Soil saturation, or wetness, of the soil is the ratio of volumetric water content to porosity:

$$\Theta = \frac{\theta}{\phi} \quad (5)$$

where

$$\begin{aligned}\Theta &= \text{soil saturation [-]} \\ \theta &= \text{volumetric water content [-]} \\ \phi &= \text{porosity [-]}\end{aligned}$$

Due to the permanent residual water content described above it is useful to define the effective saturation:

$$\theta^* = \frac{\theta - \theta_r}{\phi - \theta_r} \quad (6)$$

where

$$\begin{aligned}\theta^* &= \text{effective saturation [-]} \\ \theta &= \text{volumetric water content [-]} \\ \theta_r &= \text{permanent residual water content [-]} \\ \phi &= \text{porosity [-]}\end{aligned}$$

The impact of saturation on infiltration characteristics has been studied by several and will be presented later.

3.1.1 Hydraulic conductivity

Hydraulic conductivity describes the ease with which fluid can move through a porous medium, given as a unit of length over time. Hydraulic conductivity is a function of fluid properties and the properties of the soil in which the fluid flows through. Looking solely at

water with a constant mass density and dynamic viscosity, hydraulic conductivity depends only on soil permeability and saturation. Permeability is a measure of a medium's ability to allow fluids to pass through it, which again depends on various soil properties. While closely related to porosity, permeability also depends on the pore shapes and how connected they are. Hydraulic conductivity is calculated as follows (Water Environment Federation and ASCE, 2012):

$$K = \frac{k \cdot \rho \cdot g}{\mu} \quad (7)$$

where

K = hydraulic conductivity [m/s]

k = permeability [m^2]

ρ = fluid density [kg/m^3]

g = gravitational acceleration [m/s^2]

μ = fluid dynamic viscosity [$N \cdot s/m^2$]

In correspondence to varying permeability, different soil types have different hydraulic conductivities, and the range of values is extremely large due mostly to the variability in grain size. Within each soil type, the variability is also large ($> 10^2$ -fold for most materials). Hydraulic conductivity estimates for common soil types are presented in Table 3.1.

Table 3.1: Hydraulic conductivities of common soil types. Adapted from Holm (2013) and Brattli (2009).

Soil type	Hydraulic conductivity [m/s]
Gravel	$10^{-1} - 10^{-3}$
Sand	$10^{-2} - 10^{-6}$
Silt	$10^{-5} - 10^{-9}$
Clay	$10^{-9} - 10^{-12}$
Gravelly till	$10^{-5} - 10^{-7}$
Sandy till	$10^{-6} - 10^{-8}$
Silty till	$10^{-7} - 10^{-9}$
Clayey till	$10^{-8} - 10^{-10}$
Till clay	$10^{-10} - 10^{-11}$

Saturated hydraulic conductivity

Infiltration is only possible if the hydraulic conductivity is sufficiently high. When the infiltration capacity is larger than the rainfall intensity, all water will be infiltrated. The infiltration capacity of a soil will decrease over the duration of a rainfall as the pore spaces are filled with water (Endresen and Sweco, 2019). As the water content in the soil approaches saturation, surface runoff increases. At soil saturation, the infiltration rate becomes constant and equal to the saturated hydraulic conductivity (K_{sat}), as shown in Figure 3.2. K_{sat} denotes the ease of water transmission at saturated conditions.

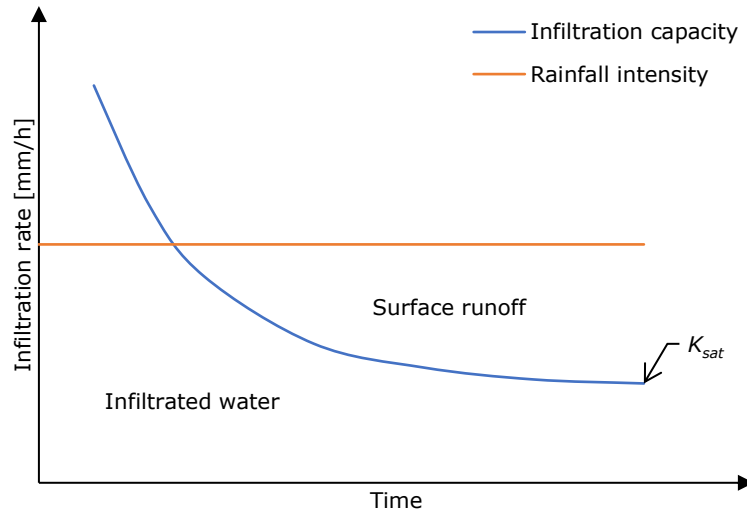


Figure 3.2: Infiltration capacity over duration of rainfall. Figure adapted from Endresen and Sweco (2019).

3.2 Formulas

Horton

The Horton Infiltration Model is one of the earliest developed infiltration models. Though several other models have been developed since then, Horton's equation is still widely used. Infiltration capacity is calculated from the following equation (Horton, 1941):

$$f_t = f_c + (f_0 - f_c)e^{-kt} \quad (8)$$

where

- f_t = infiltration capacity at time t [mm/h]
- f_0 = initial infiltration capacity [mm/h]
- f_c = final infiltration capacity [mm/h]
- k = empirical constant [h^{-1}]
- t = time since beginning of storm [h]

Van Genuchten

Van Genuchten (1980) developed a parametric model, shown in Equation (9), to describe the moisture characteristics of a soil. The relationship between water content and soil water potential can be characterized by a water retention curve. Figure 3.3 shows the water retention curve for the common soil types sand, loam, and clay based on van Genuchten parameters. The water retention curve is often applied when studying water flow in the unsaturated zone, or percolation.

$$\theta(\psi) = \theta_r + \frac{\theta_s - \theta_r}{[1 + (\alpha|\psi|)^n]^{1-\frac{1}{n}}} \quad (9)$$

where

- $\theta(\psi)$ = water retention curve [-]
- $|\psi|$ = pressure head [L]
- θ_s = saturated water content [-]
- θ_r = residual water content [-]

α = van Genuchten pressure head parameter [L^{-1}]
 n = measure of pore-size distribution [-]

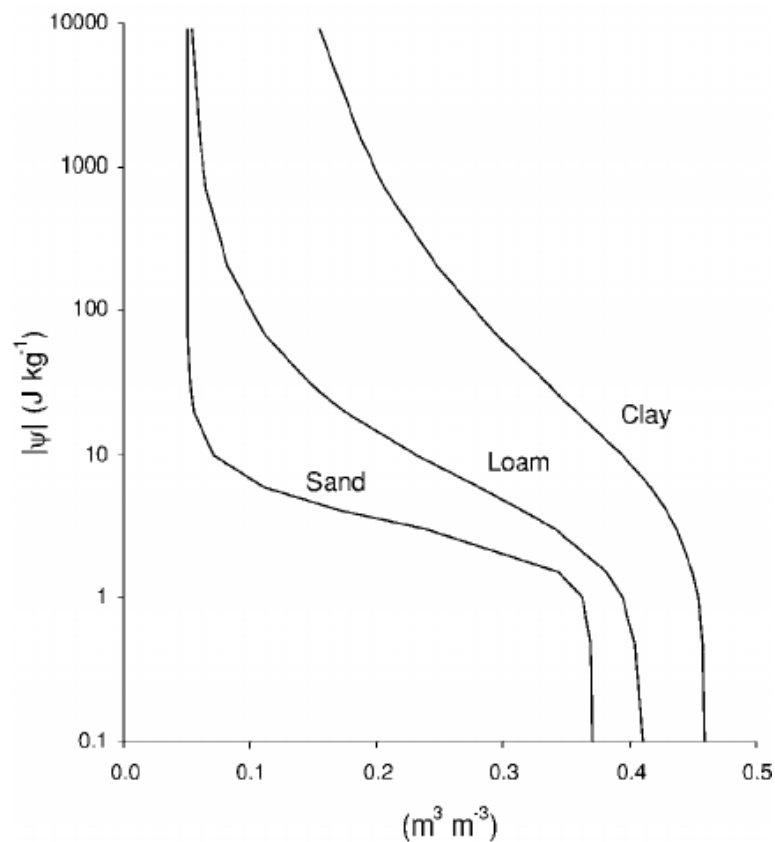


Figure 3.3: Water retention curve for sand, loam, and clay (Minasny and McBratney, 2003).

Darcy

In 1856, Henry Darcy did experiments on flow through saturated sand that led to the formulation of Darcy's law (Darcy, 1856). Darcy found that, in addition to being related to the surface area, the piezometric head, and the distance in the flow direction, flow was proportional to a constant dependent on the media properties. This constant, the hydraulic conductivity, was described in Section 3.1.1. In other words, Darcy's law describes the fluid flow through a porous medium and can be applied to both infiltration and percolation calculations. Downward unsaturated flow through a uniform soil matrix can be described as follows (Dingman, 2015):

$$Q = -K \cdot A \cdot \frac{\Delta h}{\Delta l} \quad (10)$$

where

- Q = flow [m^3/s]
- K = hydraulic conductivity [m/s]
- A = surface area for infiltration/percolation [m^2]
- Δh = piezometric head [m]
- Δl = distance in direction of flow [m]

A simplified version of Darcy's law is sometimes used when Δh and Δl are unknown:

$$Q = K_{sat} \cdot A \quad (11)$$

where

Q = flow [m^3/s]

K_{sat} = saturated hydraulic conductivity [m/s]

A = effective area for infiltration/percolation [m^2]

3.3 Dimensioning of infiltration systems

Knowledge of local soil characteristics is essential when designing infiltration systems. Infiltration capacity is particularly important, as it is a determining factor for the suitability of local SWM solutions. According to Holm (2013), soils with an infiltration capacity between 10^{-3} and 10^{-6} m/s are normally suited for infiltration purposes. An infiltration capacity above 10^{-3} will be too high for effective pollutant removal, although pollution control is not a topic of discussion in the current study. A simplified method for calculating the infiltration capacity of an infiltration system is the following (Multiconsult, 2018a):

$$Q_{inf} = k_f \cdot w \cdot l \quad (12)$$

where

Q_{inf} = system infiltration capacity [m^3/s]

k_f = soil infiltration capacity [m/s]

w = width of infiltration system [m]

l = length of infiltration system [m]

With an approximate k_f from soil condition knowledge and a Q_{inf} requirement in place, the necessary area of the infiltration system can be decided upon.

3.4 Urbanization impacts

Though implementing measures to increase urban infiltration has several benefits, caution must be taken. The hydraulic conductivity of a soil can decrease as a result of compaction and siltation (Endresen and Sweco, 2019). Current regulations therefore recommend that future infiltration properties are evaluated before potential infiltration facilities are built. Establishing infiltration systems in places with unsatisfactory infiltration capacity may lead to flooding and structural damages. A number of related challenges have been identified and studied in previous research. The effects of urbanization alter infiltration properties, making the long-term efficiency of such measures uncertain.

Prior studies show that soil degradation impairs infiltration properties, and that compaction due to urbanization is a substantial contributor to this (Pitt, Chen and Clark, 2002; Yang and Zhang, 2011). Construction activities, heavy traffic, and everyday use are all factors that contribute to reduced infiltration capacity. Subsequently, higher surface runoff may occur. Ultimately, research by Pitt *et al.* (1999), Pitt, Chen and Clark (2002), Gregory *et al.* (2006), and Yang and Zhang (2011) show that higher levels of soil compaction correspond to low infiltration capacity. According to Pitt *et al.* (1999), traditional infiltration models do not consider the effects of compaction, and they argue that compacted soils behave differently from what such models predict. Determining K_{sat} values from soil-maps, drilling samples and sieving analysis may fail to consider the effects of compaction (Aas and Muthanna, 2017), and result in significant errors in estimated infiltration rates.

In addition to compaction level, soil type and saturation also play a role in stormwater infiltration. Field capacity and soil moisture content collectively determine the volume of infiltrated stormwater (Water Environment Federation and ASCE, 2012). However, studies show that while saturation has little effect on the infiltration rate in sandy soils, clayey soils are significantly affected by saturation level (Pitt, Chen and Clark, 2002; Pitt *et al.*, 1999). Ultimately, the available pore space for water storage is decisive for infiltration capacity.

3.4.1 Urban karst

Urban soils are often distributed by various underground infrastructures, such as pipes, high permeability trenches, and other excavations. High porosity and large voids may result in higher hydraulic conductivities than surrounding soils (Sharp and Garcia-Fresca, 2003), creating preferential paths for infiltrated stormwater. This less-studied phenomenon is known as “urban karst” and was first described by Kaushal and Belt (2012). Urban karst refers to the system of underground pipes and trenches that interacts with subsurface flows and infiltration (Bonneau *et al.*, 2017), and is illustrated in Figure 3.4. G is the stormwater infiltration system receiving runoff from an impervious area (A). C and D represent elements of the urban karst, respectively pipes/telecommunications and associated trenches with backfill materials. E is the expected pathway of infiltrated stormwater to the receiving water (F). B represents the possible shortcuts the infiltrated stormwater may travel.

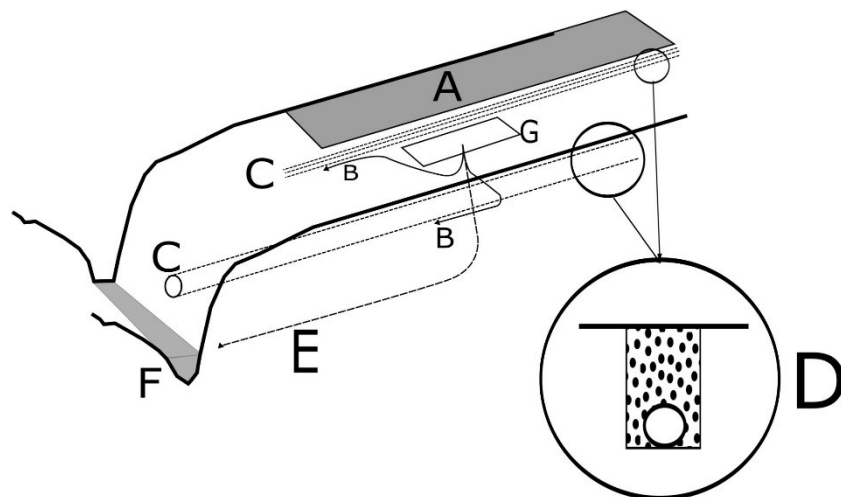


Figure 3.4: Urban karst principle (Bonneau *et al.*, 2017).

With uncertain subsurface flow paths, accurately measuring infiltration is difficult, as observed by Aas and Muthanna (2017). This could undermine attempts to restore natural flow regimes through infiltration-based LID systems (Bonneau *et al.*, 2017). Stormwater infiltration systems are often placed within meters of underground infrastructure in today’s urban streetscapes, making urban karst inevitable.

3.5 Climatic impacts

A topic of concern to infiltration performance is cold climate conditions and freeze-thaw cycles. Though low temperatures have been linked to lowered infiltration capacity, several studies still imply that infiltration is a suitable means of SWM in cold regions. Findings from studies on cold-climate impacts on different infiltration-based stormwater controls are presented in the following.

Permeable pavements

Studies by Roseen *et al.* (2012) show no consistent variations in seasonal hydrological performance of cold-climate porous asphalt. Although correlation between temperature and infiltration capacity was observed at some locations, it appeared that climatic conditions were not the main reasons for infiltration capacity degradation. Rather, clogging due to the lack of maintenance and the application of de-icing agents and anti-slip materials appeared to be degrading infiltration capacity substantially, as supported by Huang *et al.* (2016) and Al-Rubaei *et al.* (2013).

Bioretention

Studies show that cold-climate bioretention cells with low K_{sat} values can be subject to significant seasonal variability in hydrologic performance and perform poorly with regards to infiltration (Paus, Muthanna and Braskerud, 2016). In contrast, cells with low K_{sat} in the latter study infiltrated nearly all the incoming runoff. The authors therefore suggest targeting a high K_{sat} value (> 10 cm/h) when designing bioretention cells for use in cold-climate regions to ensure optimal hydrologic performance.

Amended filters

Low temperatures has been observed to be related to decreased infiltration rate in adsorbent amended filters and low unfrozen water content percentage (Monrabal-Martinez *et al.*, 2019). However, the adsorbent amended filters in the latter study preformed well under partially frozen conditions and were considered suitable for SWM in cold-climate conditions, despite the infiltration detriment.

4 Description of pilot

4.1 Site description

Trondheim is located in mid-Norway at the southern part of the Trondheim fjord, as shown in Figure 4.1. Trondheim has a coastal climate with an average yearly temperature of 5.5°C and a precipitation average of 950 mm per year (Norsk Klimaservicesenter, 2016). Both temperature and yearly precipitation are expected to increase over time. Much of Trondheim is situated on clayey soils and marine depositions, yet the top soil layers in the city centre consists mostly of backfill materials (NGU, 2019). As illustrated in Figure 4.2, the area is relatively densely developed and is primarily used for urban purposes, such as commerce, hotels, and restaurants, in addition to being home to some residential buildings.



Figure 4.1: Geographical location of Trondheim. Illustration created in Kartverket (2020b).



Figure 4.2: Satellite photo of Trondheim city centre (Kartverket, 2020a).

4.1.1 Ground conditions

Ground conditions are assessed through a review of reports from prior core drillings at the study site. Internal reports from Trondheim municipality are accessible through an online service, while reports by external commissioners must be purchased. Nonetheless, reports from projects where Trondheim municipality was the employer have been made accessible upon request. The reports used in this study are listed in Table 4.1.

Table 4.1: Geotechnical reports on Trondheim town square.

Report number	Report name ¹	Year	Commissioner
0200	Kongens gate – core drillings	1970	Trondheim municipality
1129	Trondheim Town square – core drillings	2001	Trondheim municipality
417316	Geotechnical soil surveys	2018	Multiconsult

¹ English translation of original name

Although several soil drillings have been conducted at the town square, few deep drillings are available. The drillings from 1970 and 2001 are only approximately 3 m in depth. Multiconsult performed supplementary drillings in 2018 in order to document and confirm the previous findings. Figure 4.3 shows the location of the drilling points, with the respective report number written in parenthesis.

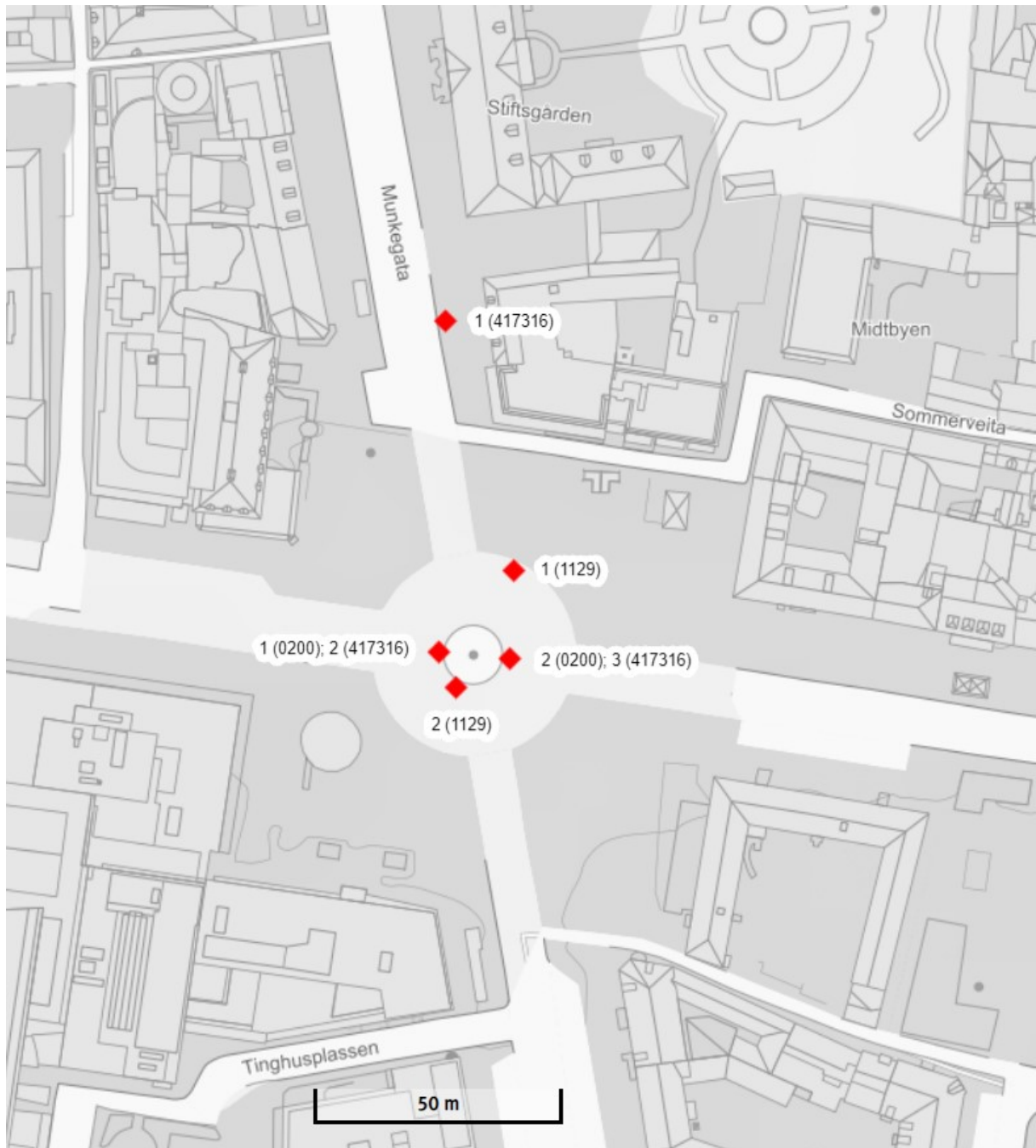


Figure 4.3: Location of drilling points. Illustration created in Kartverket (2020b).

A total of 12 core drillings are presented in Report 0200 (Trondheim kommune, 1970). Drilling points 1 to 3 are of primary interest as these are situated on the town square. The remainder of the drilling points (not displayed in Figure 4.3) are in Kongens gate, east of the town square and are less relevant for the current study. A spiral drill was used for all the drillings. Samples were taken every $\frac{1}{2}$ m in depth, and to reduce the risk of false findings only the lower part of the samples were used in analysis. The results are presented in Table 4.2: Results from Report 0200. Adapted from Trondheim kommune (1970). Table 4.2. The topset bed at point 2 consists of 1.5 m humic sand, while at points 1 and 3 a cultural layer with unspecified soil contents was found in the top 1 and 1.25 m, respectively. Below this, all three samples consist of silty sand.

Table 4.2: Results from Report 0200. Adapted from Trondheim kommune (1970).

Drilling point	Soil type	Depth below surface [m]
1	Unspecified cultural layer	0 – 1
	Silty sand	1 – 2
2	Humic sand	0 – 1.5
	Silty sand	1.5 – 3.5
3	Unspecified cultural layer	0 – 1.25
	Silty sand	1.25 – 3.25

Drilling points 1 and 2 from Report 1129 (Trondheim kommune, 2001) are of interest, although the samples are of limited depth (approximately 3 m). A screw drill was used for the drillings, and the results are presented in Table 4.3. The ground consists of 0.5 m sandy gravel over a 0.3 to 0.5 m cultural layer consisting of humic sand. The humus content in the cultural layer is said to be very low and barely measurable. Below this, gravel was found, transitioning to sand and silt at greater depths. Water content was in range 3 to 20%. The groundwater table was assumed to be at least 7 m below the ground surface, corresponding to approximately 2.1 and 2.4 m.a.s.l. (meters above sea level) at drilling point 1 and 2, respectively.

Table 4.3: Results from Report 1129. Adapted from Trondheim kommune (2001).

Drilling point	Soil type	Depth below surface [m]
1	Sandy gravel	0 – 0.5
	Humic/sandy cultural layer	0.5 – 0.75
	Medium sand	0.75 – 1
	Fine gravel	1 – 2
	Fine sand	2 – 3
2	Sandy gravel	0 – 0.5
	Humic/sandy cultural layer	0.5 – 1
	Fine gravel	1 – 2
	Fine/medium sand	2 – 3
	Sandy sand	N/A

Rotary pressure sounding was performed by Multiconsult (2018b) at points 1, 2, and 3 from Report 417316. Results from drilling 1 and 3 are displayed in Figure 4.4 and Figure 4.5, respectively. According to Emdal (2020), rotary pressure sounding is a very rough type of sounding that gives limited information about ground conditions. Yet, an estimate of soil types can be made from the shape of the resultant curve. Sounding 3 has a jagged curve typical for stratifications of solid silt and sand, and more fine-graded soils. From sounding 1 it appears that the ground closest to the infiltration facility has a topset bed consisting of friction materials above more homogenic materials at 5 to 9 m depth. Emdal (2020) suggests that this may be a cohesive soil (clay and silt mixture), but that further tests are needed to confirm this.

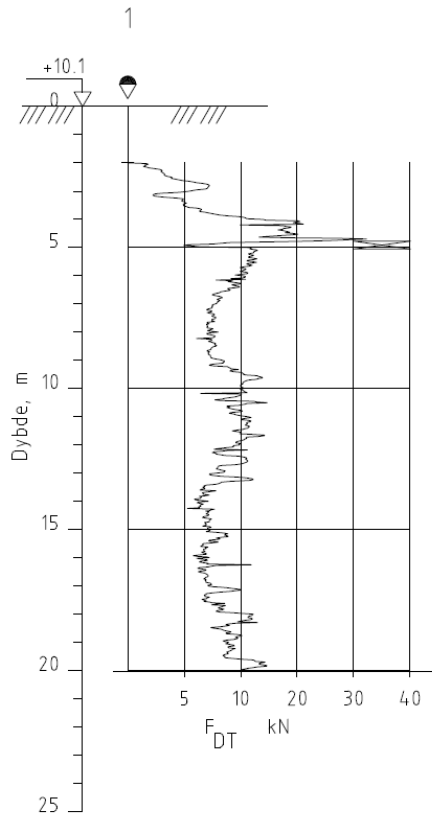


Figure 4.4: Rotary pressure sounding at point 1 (Multiconsult, 2018b).

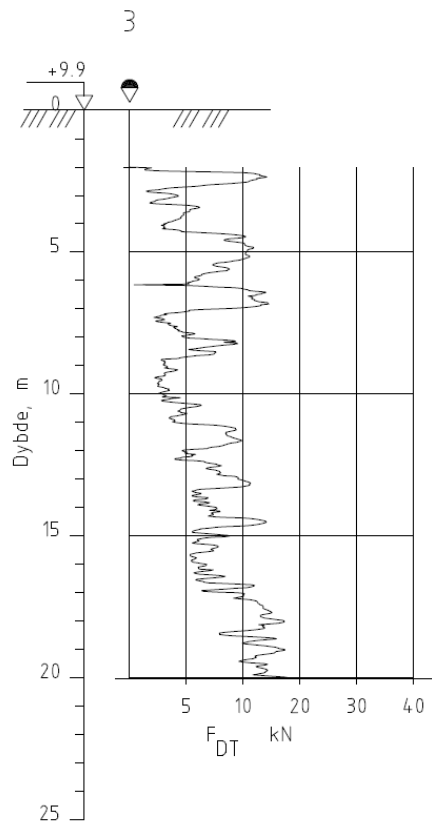


Figure 4.5: Rotary pressure sounding at point 3 (Multiconsult, 2018b).

In addition to rotary pressure sounding, a test series at drilling point 2 was obtained using 54 mm cylinder samples and bag samples (Multiconsult, 2018b). Results are displayed in Figure 4.6. Tests show that there is a 1 to 2.5 m topset bed consisting of backfill materials and cultural layers. Below this, there are stratified layers of sand and silt. Sand was found at depths between 3 and 4 m below the ground surface. Silt with elements of fine sand and clay was found at depths 4 to 10 m. Below this, the ground consists of silty and clayey sand. The water content in the sample was in the range 12.1 to 30.3%.

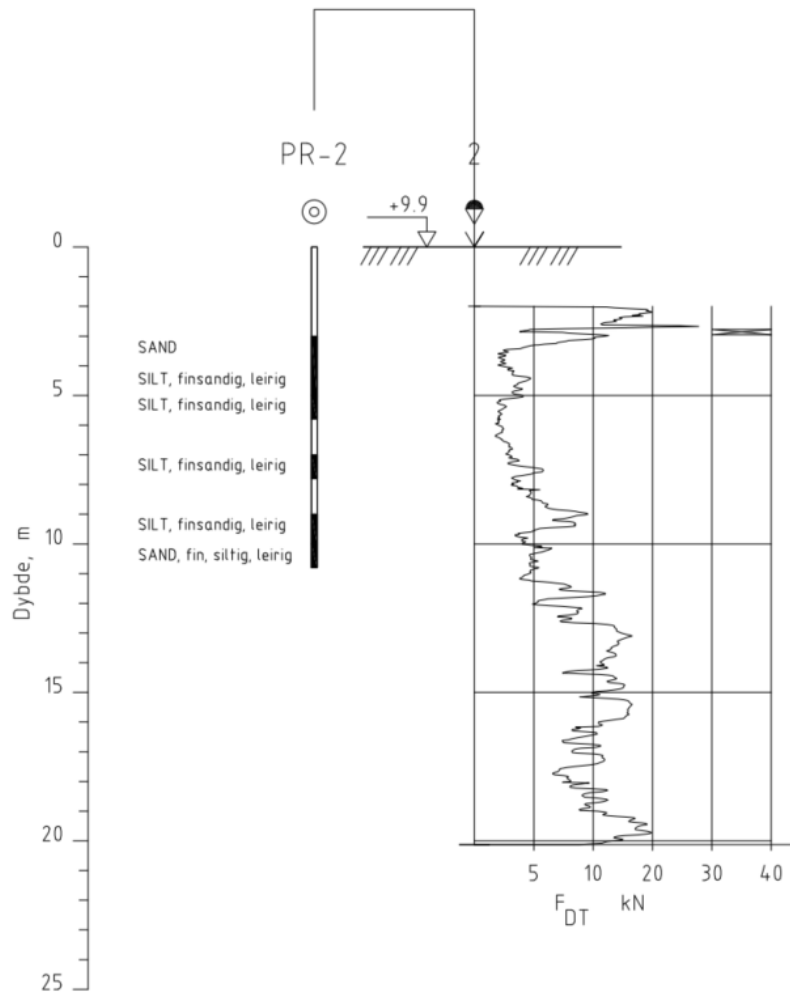


Figure 4.6: Rotary pressure sounding and soil sampling at point 2 (Multiconsult, 2018b).

4.2 Stormwater facility

The combined infiltration and detention facility studied in this thesis is located in Munkegata, just north of the town square in the city centre of Trondheim. Stormwater runoff from the town square is collected in sand-traps and transferred to the downstream infiltration facility through a piped network. A planar view of the entire stormwater system, designed by Multiconsult (2018a), is shown in Appendix 1.

Appendix 2 shows a detailed view of the infiltration facility. Stormwater runoff enters the system through manhole O17. The original design shows a continuous pipe through O17, but it was instead constructed with open-ended pipes. From distribution manhole O8 stormwater travels through four infiltration pipes and can either be infiltrated to the native

ground or transferred directly to outlet manhole O1. The infiltration pipes are 160 mm in diameter and are made from PP SN16 (Polypropylene with nominal stiffness $\geq 16 \text{ kN/m}^2$). The pipes are perforated with 300 holes per meter, each having a diameter of 8 mm.

Stormwater discharge onto the downstream piped network is regulated by a FluidVetric VSU4DN150 swirl chamber with a design capacity of 25 l/s (MFT, 2018). This is a submerged cochleate chamber with a tangential inlet directed downward. The outlet is directed normally to the chamber. Figure 4.7 illustrates the functioning of the swirl chamber at partial and completely filled conditions; at partial filling, the static pressure is low, and water flows through the outlet with low resistance. When the water level reaches the top of the chamber, an air filled whirlpool is established creating large resistance that reduces outflow (MFT, 2020).

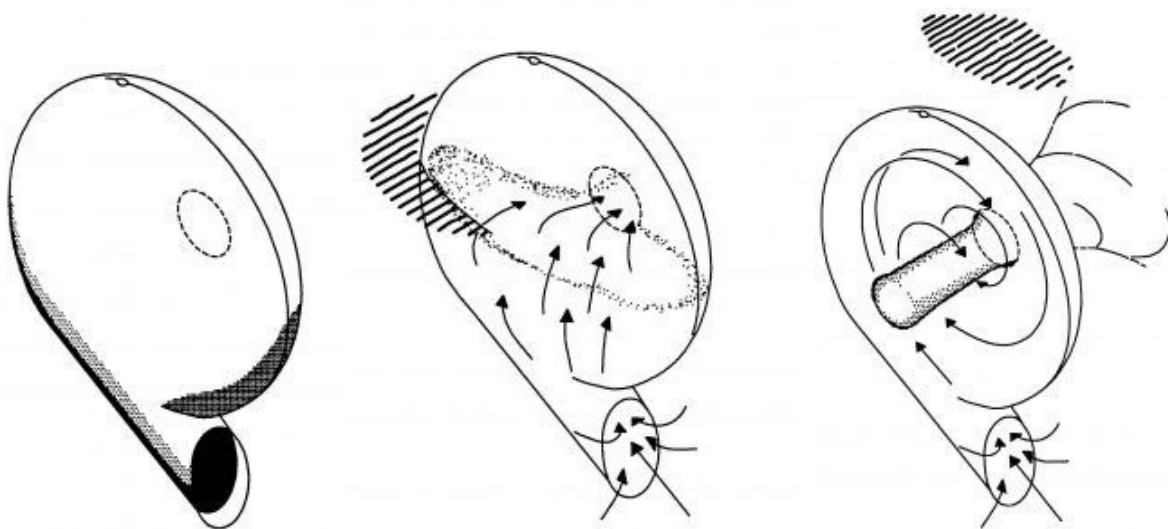


Figure 4.7: Functioning of FluidVetric VSU swirl chamber (MFT, 2020).

Three identical detention basins will be filled when the downstream discharge is exceeded or when the amount of incoming stormwater (Q_{in}) exceeds the infiltration capacity such that the water level in O8 rises above 5.20 m.a.s.l. A flow chart of the system is shown in Figure 4.8.

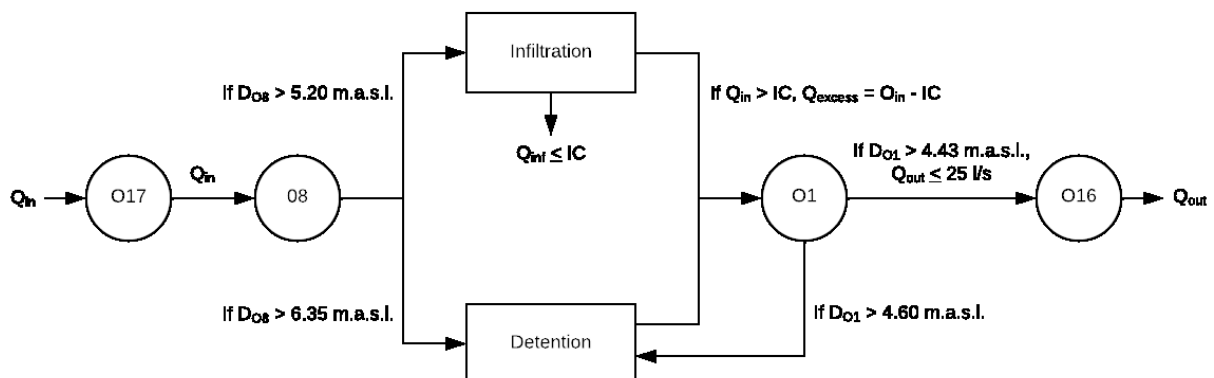


Figure 4.8: Flow chart of the infiltration and detention system.

4.2.1 Design basis

As previously mentioned, the stormwater facility was designed by Multiconsult (2018a). The facility was designed by interpreting the town square upgrading as a development project, and municipal guidelines formed the basis for design.

Drainage area

The town square is approximately 100 m by 100 m, and with the addition of corresponding areas the drainage area to the infiltration facility was estimated to 1.2 ha (12 000 m²) (Multiconsult, 2017). The amount of impermeable surfaces post upgrade is high, similar to the situation pre-upgrade, and the average runoff coefficient was set to 0.95. Reduced area, after Equation (2), is as follows:

$$A_{red} = 0.95 \cdot 1.2 \text{ ha} = 1.14 \text{ ha} = 11400 \text{ m}^2$$

Detention volume

Since the downstream piped system is combined, required detention volume is determined from Figure 2.3:

$$V = 137 \text{ m}^3$$

The system is constructed with three parallel detention basins of equal shape and size. Originally, each basin was designed with eleven Basal Q_{max}-V DN2000 ovoid concrete pipe elements (Multiconsult, 2018a), shown in Figure 4.9. Each element is 1.5 m in length and has a cross-sectional area of 2.82 m² (Basal AS, n.d.). This corresponds to a total storage volume of approximately 140 m³. However, the combined use of infiltration and detention reduces the needed storage volume, and it was decided to reduce the number of elements to eight, corresponding to a total inner length of 12 m. Subsequently, the total storage volume was reduced to 72% of the original value, equal to approximately 102 m³.



Figure 4.9: Inside of the detention basin looking north.

Infiltration

The stormwater design flow into the system was set to 400 l/s (Multiconsult, 2018a). A climate factor of 1.2 and a return period of 20 years were used in calculations. Since the system was designed prior to the ground condition assessments by Multiconsult (2018b) presented in Section 4.1.1, it was assumed that the ground consisted of single graded fine sand with $K_{sat} = 0.001$ m/s (Multiconsult, 2018a). With the original storage volume of 140 m³, the collective infiltration area was 13.6 m wide and 23.0 m in length. According to Equation (11), the infiltration capacity is:

$$\text{Infiltration capacity} = 0.001 \text{ m/s} \cdot 13.6 \text{ m} \cdot 23.0 \text{ m} = 310 \text{ l/s}$$

The reduced infiltration capacity (72% of the original value) is approximately 220 l/s.

5 Method

5.1 Data collection

Instrumentation was installed by ITAS (Scanmatic Instrument Technology AS) and Trondheim municipality, except for one CTD-diver and one Baro-diver installed by the author at a later stage. Most measured data are collected with minute resolution using a CR310 logger manufactured by Campbell Scientific (2020) and are accessed from Vista Data Vision (Vista Engineering, 2019), where it is made available for download. Data measurement techniques and equipment is explained in the following.

Inflow

Inflow to the system is measured using a Viatronics AVSS waterflow sensor in the pipe between manholes O17 and O8. This is an area-velocity flow meter that continuously measures water level and velocity to calculate flow through a pipe or open channel (Viatronics, n.d.). Water level is found by measuring the time it takes for echoes of transmitted ultrasonic pulses to return to the sensor. Velocity is found using an ultrasonic Doppler signal that is injected into the water; echoes return to the sensor after being reflected by air bubbles or particles at an altered frequency that is proportional to velocity. Output is given in m^3/s .

Water level

Water level in manholes O17 (inlet) and O1 (outlet) is measured in pressure cells using PT12 level sensors (Seametrics, n.d.). Water level is measured using a piezo-electric, media isolated pressure element. Water levels above the bottom of the manholes are given in m. Groundwater level is measured in manhole O16 using a hydraulic pore pressure sensor that measures the depth of groundwater below the ground surface. The groundwater sensor was installed on November 15th, 2018 (Trondheim kommune, 2019).

Equipment used for water level measurements inside the easterly detention basin was installed on March 10th, 2020. A CTD-diver was attached to a steel wire that was fastened to a ladder-step inside the detention basin, as shown in Figure 5.1. A CTD-diver measures hydraulic pressure in cm at the bottom of the detention basin (Van Essen Instruments, 2016). A Baro-diver is used to compensate for atmospheric pressure. It was attached to a steel wire fastened to a ladder-step above the expected maximum water level, as shown in Figure 5.2. The sample interval was set to one minute. Diver-data was collected periodically using a USB-port and Diver-Office software (Van Essen Instruments, 2019).



Figure 5.1: CTD-diver installation.



Figure 5.2: Baro-diver installation.

Water temperature

Inflow and outflow water temperatures are measured in pressure cells using PT12 sensors (Seametrics, n.d.) in manholes O17 and O1, respectively. Groundwater temperature is measured in manhole O16. Temperatures are measured using on-board digital chips and are presented in °C. The CTD-diver measures temperature of water stored in the detention basin.

Weather data

A rain gauge was planned installed on the roof of Trondheim Torg, a nearby building to the study site, but this was not possible due to the outbreak of Covid-19. Instead, precipitation data from existing weather stations were used in analysis. Weather data, thereby air temperature, dew point, snow depth, precipitation, and humidity, are collected from weather stations at Lade and Voll and accessed through Vista Data Vision (Vista Engineering, 2019). Precipitation in mm is given in both hourly and minute resolutions. Air temperature and precipitation data with minute and hourly resolutions from Risvollan and Høvringen weather stations are downloaded from the database seKlima (Norsk Klimaservicesenter, 2020).

5.2 Drainage area delineation

AutoCAD (Autodesk, 2020) was used to estimate the area draining to the infiltration system. Drainage area delineation was done by manually drawing the catchment boundary, while following the procedure described by Dingman (2015):

1. Start at the watershed outlet, in this case the inlet to the infiltration facility at O17.
2. Draw a continuous line away from O17 to the left or right.
3. Maintain the line perpendicular to the contour lines.
4. Continue the line until the trend is opposite to the direction it began.
5. Repeat step 1 to 4, but in the opposite direction of that chosen in step 2.
6. Connect the two lines at the location obtained in step 4.

The drainage area was found by using the hatch-area function in AutoCAD.

5.3 Calculation of infiltration and percolation

The infiltration rate at a given timestep is calculated by subtracting the system outflow from inflow, as follows:

$$Q_{inf} = Q_{in} - Q_{out} \quad (13)$$

where

Q_{inf} = infiltration rate [m^3/s]

Q_{in} = inflow [m^3/s]

Q_{out} = outflow [m^3/s]

The volume of inflow, outflow, and infiltrated water for each rain event is calculated by multiplying the duration, t , by Q for each timestep and adding them together:

$$V_{event} = \sum_{i=1}^n Q_i \cdot t_i \quad (14)$$

where

V_{event} = water volume [m^3]

Q_i = flow at timestep i [m^3/s]

t = duration of timestep i [s]

6 Data processing

6.1 Water levels

On March 10th, 2020, water depths were measured manually in O17 and O1 for comparison with sensor values shown in Table 6.1. This was done in two parts:

1. Depth from terrain to the water surface was measured using a laser scanner.
2. Water depth inside the manhole was measured using a folding rule.

Table 6.1: Differences in sensor and measured water levels.

Manhole	Time	Sensor water level [m]	Measured water level [m]	Error [m]	Error [%]
O17	08:40	1.162	0.19	0.972	512
O1	09:09	0.318	1.02	-0.702	69

Significant errors in water depths were found in both manholes, which must be considered when applying the data in calculations. The water level measurements in O17 may be used for comparison with inflow but say little about system performance with respect to detention basin usage and infiltration. Thus, the measurements are of limited importance to this study. The water level in O1 is however essential in outflow calculations, and the measurement errors are unfortunate. Sensor calibration was originally planned but was unfeasible at the time due to Covid-19. Therefore, instead of applying the sensor water level directly, the stable water level during periods without precipitation and no expected in- or outflow was determined. The variation in water level was determined by subtracting the stable dry weather water level from the measured water level at each timestep.

6.2 Inflow

6.2.1 Noise

Inflow data show unwanted noise during periods assumed to have constant flow. Noise was in this study defined as follows:

If $x_t \equiv x_{t+u}$ and $x_{t+1}:x_{t+(u-1)} \neq x_t$, then $x_{t+1}:x_{t+(u-1)}$ are considered as noise.

This can be described in wording:

If the measured value at time 1 is equal to the measured value at the time a given number of timesteps later, and the values between time 1 and u do not equal the value at time 1, then the values between time 1 and u are considered as noise.

x is the measured inflow data. u is a predefined integer that describes the maximum number of timesteps between two equal measured data values in order for the in-between values to be considered as noise. Noise is filtered out by setting $x_{t+1}:x_{t+(u-1)}$ equal to x_t .

The programming language R was used to make a program that filters out unwanted noise. The complete code is shown in Appendix 3 and described in wording below.

1. x_t is compared to x_{t+j} , where $j \in [2, u]$.

2. If $x_t \equiv x_{t+j}$, then any value of $x \neq x_t$ in the time interval $[t + 1, t + j - 1]$ will be set equal to x_t .
3. If $x_t \neq x_{t+j}$, j is increased by one and the loop will return to step 1.
4. The loop continues onto the next timestep, $t + 1$, and repeats steps 1 to 3 until the end of the dataset.

In the current study u is set to 5, meaning that up to four values between two equal measurements may be considered as noise. For instance, if $x_t \equiv x_{t+3}$, two in-between values may be considered as noise and changed to equal x_t . Similarly, if $x_t \equiv x_{t+5}$, four in-between values may be changed.

6.2.2 Threshold level

Following periods without precipitation it is expected that there is no inflow to the system. However, graphical analysis show that the collected inflow data is not in accordance to this presumption; following precipitation events the inflow stabilized at approximately 6 l/s, and not at zero as expected. Thus, it appears that the threshold for zero inflow was incorrect. To improve data quality and avoid falsely high inflow data, all data measurements were adjusted accordingly.

6.3 Outflow

Outflow values are determined from calculations by MFT (2018) on hydraulic characteristics of the swirl chamber for various water levels. Water level above the centre line of the outlet orifice and corresponding outflow are included in Appendix 4. The orifice nozzle is 199 ± 1 mm in diameter, meaning the centre line is approximately 100 mm above the nozzle threshold. The threshold level is assumed to be equal to the stable water level in O1 during dry periods. The total head above the centre line (h_r) is calculated as follows:

$$h_r = \text{measured water level} - \text{stable dry weather water level} - 100 \text{ mm} \quad (15)$$

h_r is finally used to determine the outflow Q_{out} at each timestep using linear interpolation.

6.3.1 Outflow at low water levels

According to Aaby (2020) outflow through the swirl chamber is uncertain at low water levels. As displayed in Figure 6.1, outflow is most uncertain for partial filling with an uncertainty assumed to be at least 40%. Though outflow is less uncertain when the swirl chamber is partially submerged, the flow is turbulent, and the uncertainty is still assumed to be at least 20%. The outflow is most certain when the entire swirl chamber is underwater, and the whirlpool is fully established. At h_r higher than 0.3 m, the uncertainty is 10% (MFT, 2018).

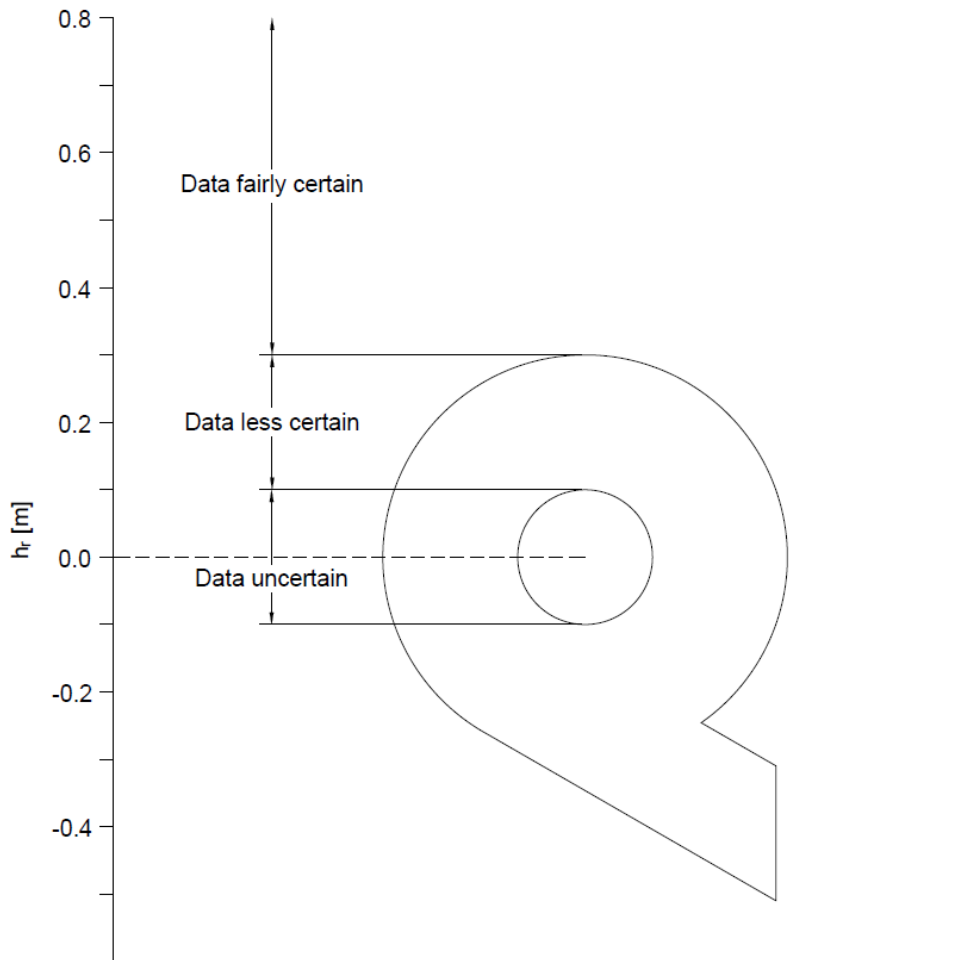


Figure 6.1: Uncertainty of outflow from swirl chamber. Adapted from Aaby (2020).

A portion of the measured water levels are below the orifice centre line, but still above the nozzle threshold. No outflow values are available for water levels in this range and must therefore be calculated by other means. Aaby (2020) recommends considering pressure loss when calculating outflow. hd is the pressure loss through the swirl chamber inlet and hw is the pressure loss over the nozzle threshold. The water level above the nozzle threshold, h' , is the sum of hd and hw , as shown in Figure 6.2. h' equals $h_r + 100$ mm. At $h_r = 0.003$ m, which is the lowest calculated water level by MFT (2018), $h' = 0.103$ m and $Q = 2.26$ l/s.

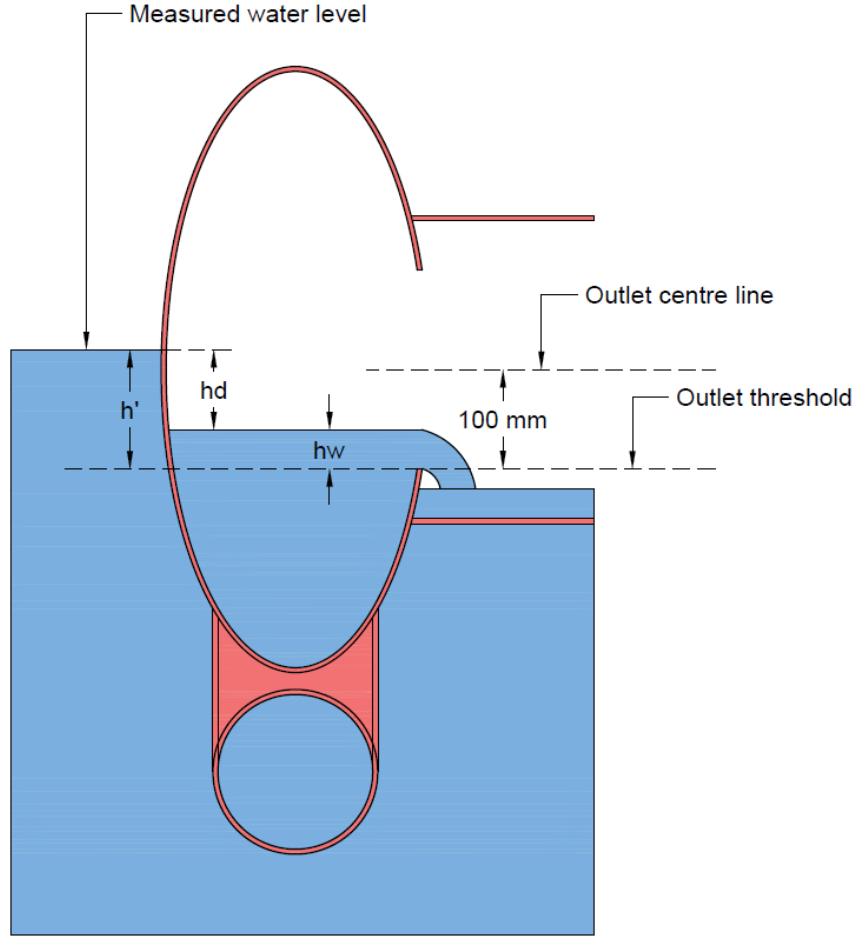


Figure 6.2: Water level references in swirl chamber. Adapted from Aaby (2020).

h_w is estimated from Equation (16) (Vatankhah, 2016):

$$Q_w = 0.79 \cdot C_w \cdot \eta^2 \cdot \sqrt{2g \cdot D^5 \cdot (1 - 0.54\eta)} \quad (16)$$

where

$$\begin{aligned} Q_w &= \text{flow across weir [m}^3/\text{s]} \\ C_w &= \text{weir discharge coefficient [-]} \\ D &= \text{outlet diameter [m]} \\ g &= \text{gravitational acceleration [m/s}^2\text{]} \\ \eta &= \frac{h_w}{D} \text{ [-]} \end{aligned}$$

C_w was set to 0.7, as suggested by Aaby (2020). η and Q_w were then calculated for a range of h_w -values. Linear interpolation shows that at $Q = 2.26$ l/s, $h_w = 0.047$ m. hd was estimated using Torricelli's law (Aaby, 2020), discovered by the Italian physicist Evangelista Torricelli in 1643:

$$Q_d = \mu \cdot A \cdot \sqrt{2g \cdot hd} \quad (17)$$

where

$$\begin{aligned} Q_d &= \text{inflow to swirl chamber [m}^3/\text{s]} \\ \mu &= \text{flow coefficient [-]} \end{aligned}$$

A = cross sectional area of inlet [m^2]
 g = gravitational acceleration [m/s^2]
 hd = pressure loss through swirl chamber inlet [m]

Cross-sectional area of a circular pipe is calculated as follows:

$$A = \frac{1}{4} \cdot \pi \cdot D^2 \quad (18)$$

where

A = cross-sectional area [m^2]
 D = pipe diameter [m]

The inlet diameter is 150 mm. Applying Equation (18) the cross-sectional area of the inlet is 0.01767 m^2 . At $Q_{out} = 2.26 \text{ l/s}$, $hd = h' - h_w = 0.103 - 0.047 = 0.056 \text{ m}$. μ was determined from $Q_{out} = 2.26 \text{ l/s}$ and the corresponding value of hd :

$$\mu = \frac{Q_{out}}{A \cdot \sqrt{2g \cdot hd}} = 0.1217$$

Q_d was then calculated for a range of hd -values, and h' determined for a range of outflow-values. The result is graphically displayed Figure 6.3. Q_{out} was finally determined from measured h' using linear interpolation.

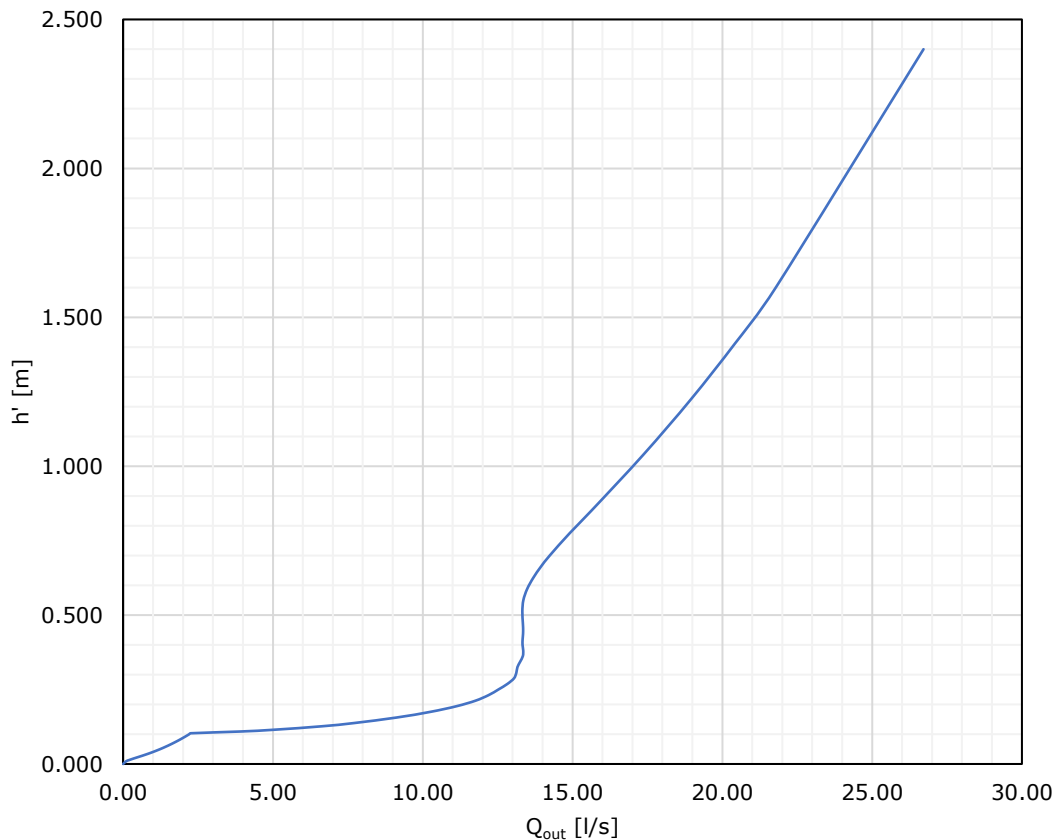


Figure 6.3: Outflow response to different water levels.

7 Results and discussion

7.1 Drainage area

Delineation of the elevation plan in AutoCAD using the method described in Section 5.2 resulted in a calculated drainage area of 6042 m². The drainage area is shaded in red in Figure 7.1. The drainage area described by Multiconsult (2017) was 1.2 ha. This is approximately twice the area found from delineation. Several factors contribute to this difference.

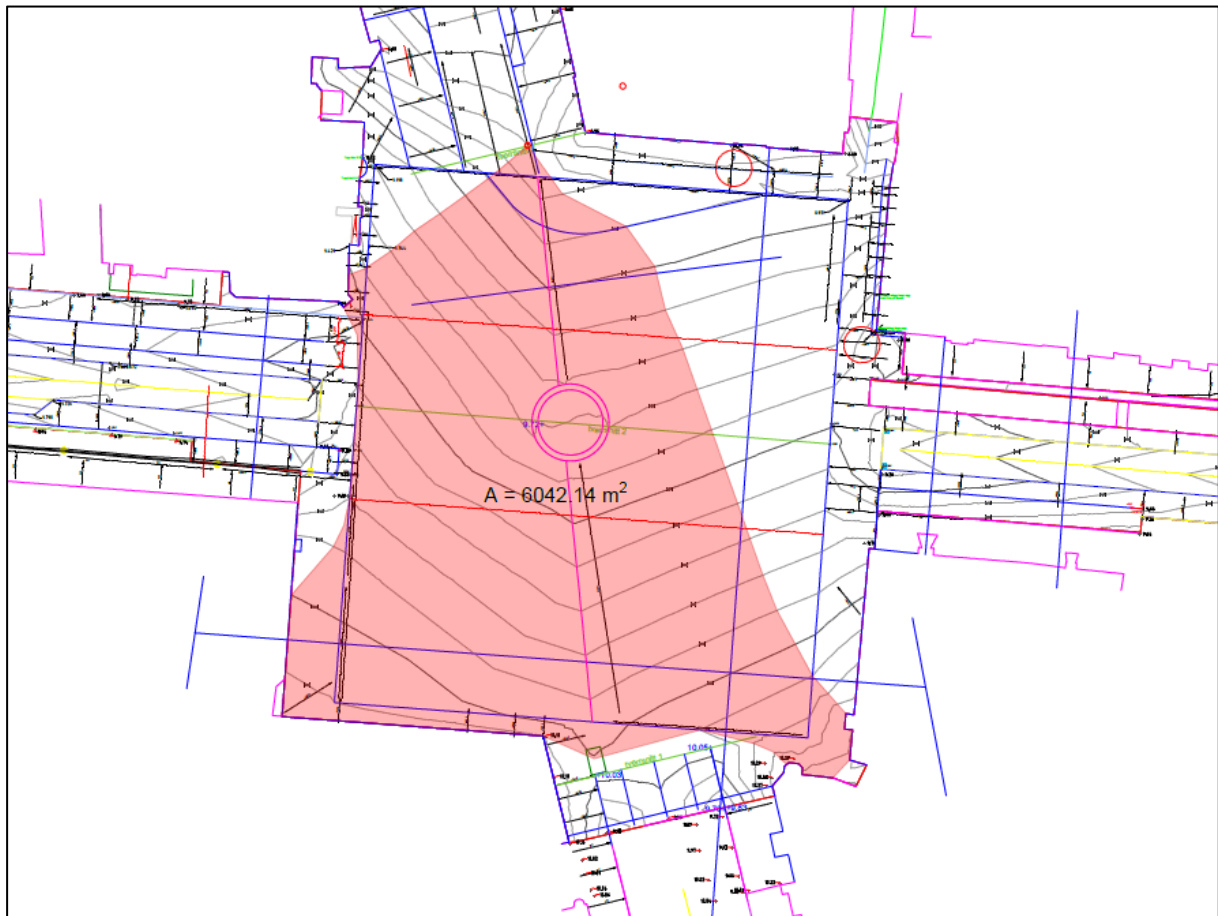


Figure 7.1: Drainage area from delineation.

The most apparent reason why the drainage area in Multiconsult (2017) is higher is because the entire town square surface, in addition to parts of the adjacent streets, were included. This evaluation was likely done prior to the finalization of the elevation plan, as the elevation plan is dated 14.12.2017. It appears that the drainage area in Multiconsult (2017) was based on the existing terrain at the time, in which the adjacent streets did not slope away from the town square surface.

Secondly, Multiconsult (2017) does not separate the drainage area to the combined infiltration- and detention system from the drainage area to infiltration-trench in the northwestern part of the town square. Since the infiltration trench does not have an available detention volume, the municipal guidelines described in Section 2.1.1 could not

be directly applied. This might be the reason why the entire town square surface was included when calculating the detention volume in the combined infiltration- and detention system. Uncertainty in the size and nature of future precipitation events due to climate change, in combination with the 100-year excavation restriction on site might also have resulted in a more conservative approach to design.

Moreover, the actual drainage area is still uncertain, as the elevation plan is purely theoretical. Inaccuracies in construction work, potential frost heave, and various landscape components may affect the nature of the town square surface and hence influence the drainage area and drainage patterns. A more thorough analysis of the post-development terrain would be required to get accurate runoff characteristics, for example by creating a digital elevation model (DEM) from a laser-scan of the terrain. The DEM can be analysed using GIS (Geographic Information System) software.

7.2 Analysis of collected data

A significant part of this study has revolved around data analysis and processing. In the following, the processed data will be presented and analysed. The complete graphs of the respective data are shown in Appendix 5 to 10.

7.2.1 Precipitation

As described, precipitation data from a number of weather stations were collected and considered for analysis. The precipitation data series from Lade and Høvringen have extended periods with missing data and were therefore excluded from the current study. While the data series from Voll and Risvollan are complete, neither of the weather stations are near the study site. Voll is situated 127 m.a.s.l. approximately 3.5 km in aerial distance from the study site. While being roughly the same aerial distance from the town square, Risvollan is situated at 84 m.a.s.l. It was ultimately decided that the Risvollan data series was most suitable to the current study. The complete graph of hourly precipitation data at Risvollan is shown in Appendix 5 and air temperature data in Appendix 6. The total precipitation volume from February 1st to May 14th is approximately 2014 m³.

Accurate precipitation data is essential in precipitation volume calculations. Hence, the distance from the weather station to the study site is likely a major source of error in this case. Differences in precipitation patterns and amounts may vary locally, and although data from Risvollan is similar to those from other weather stations in Trondheim, it is difficult to know whether these data can be applied to the study site with certainty. Precipitation measurements closer to the study site would have been preferred with respect to data quality. A simple rain gauge may be installed on the roof of one of the nearby buildings to improve data quality in future work. This way, the rain gauge is shielded from the general public that traffic the town square.

7.2.2 Inflow

The complete graph of processed inflow data is shown in Appendix 7. Data is missing from 15:29 on April 23rd to 09:08 on April 30th, possibly due to silt or other substances covering the flow sensor. Excluding this period from calculations gives a precipitation volume of 1981 m³. The total inflow volume from February 1st to May 14th, excluding the period with missing data, is approximately 1855 m³. This is slightly less than the precipitation volume but is within a reasonable range; the difference can likely be explained by uncertainties in inflow data processing or uncertainties related to precipitation patterns and drainage area, as explained previously. In addition, some precipitation volume may be lost to

evapotranspiration prior to reaching the system inlet. The data processing also results in somewhat angular patterned graphs that are poorly suited for visual interpretation of inflow patterns. Nonetheless, the accuracy of the flow meter is likely different for various flow levels and adjusting all data equally may therefore not be optimal and in some cases have unfortunate effects on the results.

7.2.3 Outflow

The complete graph of calculated outflow data based on the procedure explained in Section 6.3 is shown in Appendix 8. The total outflow volume from February 1st to May 14th is approximately 1673 m³. When excluding the measurements from the period with missing inflow data the volume is changed by less than 1 m³. The outflow volume is 182 m³ less than the total inflow volume for the same period, which implies that some inflow volume was retained through infiltration to the ground. Looking at the facility as an isolated system, it is reasonable to expect that outflow volume is less than the inflow. Yet, the high uncertainty in outflow for low water levels, as well as the uncertainty in inflow, complicates the comparison of the two and one cannot be certain that the difference in volumes is real. As explained in Section 3.4.1, infiltrated stormwater tends to find preferential subsurface paths and runoff may also have entered the system through small openings or vents downstream of the inflow sensor.

7.3 Analysis of rain events

Six significant rain events are analysed further in the following. Graph patterns are analysed, and inflow, outflow, infiltration, and precipitation volumes are compared. The precipitation data and temperatures are from the Risvollan weather station.

Event 1: February 2nd, 2020

The first significant rain event occurred during the morning and early afternoon on February 2nd. The results are displayed in Table 7.1 and Figure 7.2. The total precipitation was 19.8 mm with a calculated volume of 119.63 m³. The precipitation peak of 3.9 mm occurred between 04:00 and 05:00. Inflow, outflow, and infiltration volumes from Equation (14) are 92.16, 205.83, and 4.52 m³, respectively. The temperature was low but remained above the freezing point for the duration of the rainfall. The highest registered temperature was 2.5°C at 11:00.

Table 7.1: Results from Event 1.

	Volume [m³]	Peak flow [l/s]	Time of peak
Precipitation	119.63		
Inflow	92.16	10.00	02.02.2020 05:13
Outflow	205.83	10.02	02.02.2020 05:10
Infiltration	4.52	0.78	02.02.2020 19:37

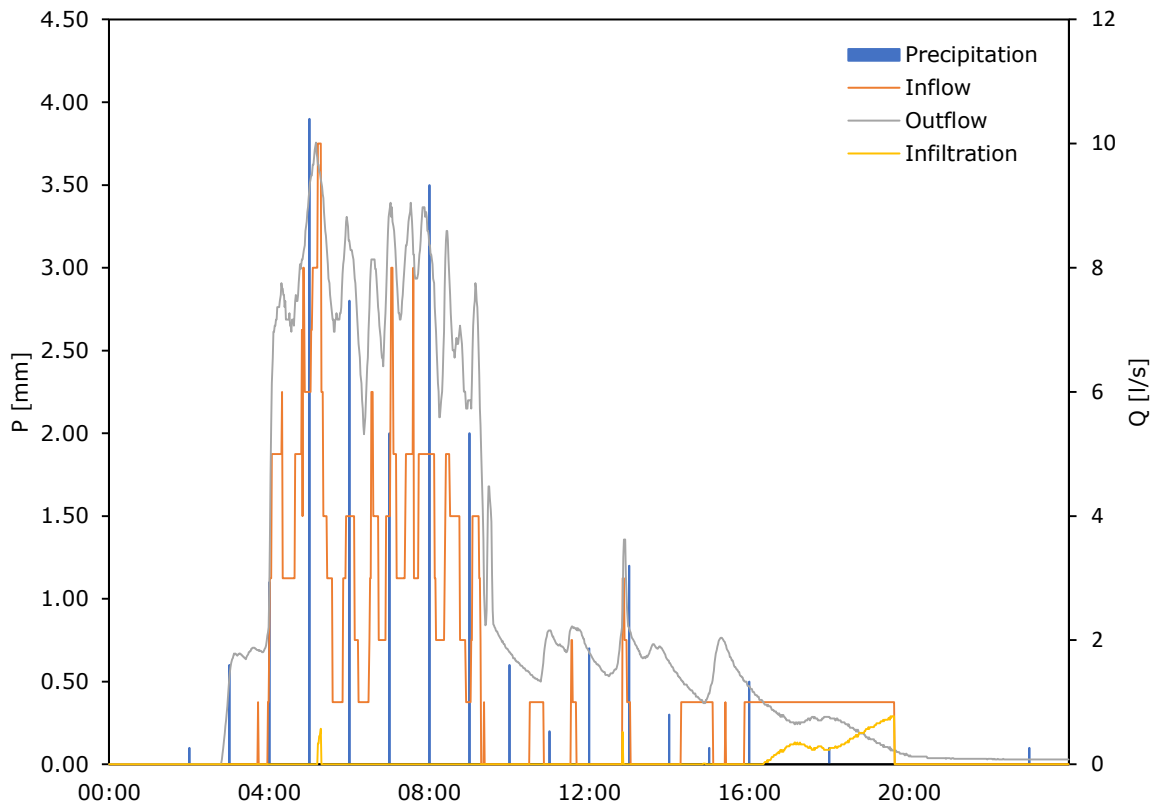


Figure 7.2: Results from Event 1.

As expected, inflow increases as runoff starts to accumulate. The peak inflow of 10.00 l/s occurs just after the precipitation peak. Inflow fluctuates in the succeeding hours until it finally stabilizes at 0 l/s by the end of the rain event.

Interestingly, it appears that outflow starts to increase prior to inflow. In accordance with increased precipitation, outflow rapidly increases. Outflow fluctuates for about four hours followed by a gradual decrease at the end of the rain event. Moreover, the outflow volume is substantially higher than both inflow and precipitation volumes. Urban karst may to some extent explain why outflow exceeds inflow, but the difference from precipitation volume is unlikely high and is therefore regarded as false. Uncertainty at several levels may contribute to this error.

Infiltration appears to be low for the studied rain event. However, this is most likely a result of the elevated outflow calculations and it is expected that infiltration in reality is substantially higher. However, several factors may contribute to low infiltration including clogging of the infiltration pipes, saturation in the subgrade soil and climatic impacts. The infiltration peak at 19:37 appears to be caused by imperfections in the inflow data processing since precipitation is minimal at this time. Since the level sensor in the detention basin were not installed at the time, the amount of stored stormwater is uncertain. Due to the elevated water level in O1 at the time it is presumable that the detention basins were utilized.

Event 2: February 4th – 6th, 2020

The second significant event lasted from February 4th to February 6th. This event is the largest in size in the data series, totalling 58.70 mm. The total volume was 354.67 m³ with a peak precipitation of 4.7 mm between 14:00 and 15:00 on February 5th. The results are

displayed in Table 7.2 and Figure 7.3. The air temperature was above the freezing point for the beginning of the rain event, but from 23:00 on February 5th to 20:00 the next day the air temperature was just below the freezing point. This may have resulted in freezing rain and will be discussed further in the following.

Table 7.2: Results from Event 2.

	Volume [m ³]	Peak flow [l/s]	Time of peak
Precipitation	354.67		
Inflow	151.86	17.00	05.02.2020 13:56
Outflow	244.18	10.67	05.02.2020 13:59
Infiltration	35.73	6.47	05.02.2020 13:56

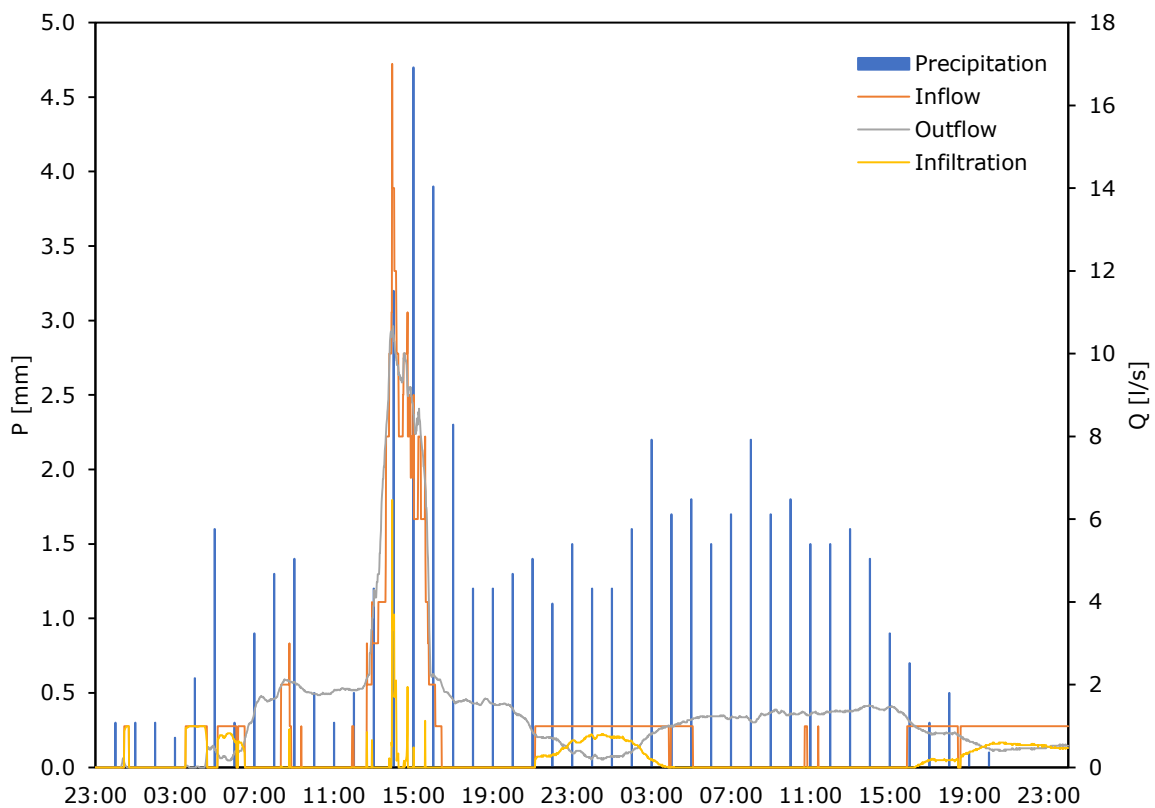


Figure 7.3: Results from Event 2.

Similar to Event 1 outflow volume exceeds inflow volume and may be influenced by the same factors explained above. It is also possible that the calculated inflow is too low due to inaccuracies in the flow meter and the data processing. However, in this case precipitation continues far longer than the elevated in- and outflow levels, which explains why the cumulative precipitation volume is significantly higher. The most probable explanation is local differences in precipitation patterns as described in Section 7.2.1. Since the inflow peak occurs prior to the precipitation peak, a delay between rainfall at the study site and the measurement station is likely. It also appears that the majority of the rainfall was local at Risvollan, and hence had little impact on the hydrology on site. Alternatively, the low air temperature could have caused freezing rain at the study site; low surface temperature may cause rain to freeze upon reaching on the ground. When this happens, the measured precipitation in the rain gauge will differ from runoff volume since rain is stored as ice on the ground surface.

Infiltration was present to a larger degree than the previous event with a peak of 6.47 l/s. According to the graph, infiltration decreases quickly after the peak, when in- and outflow are practically equal. The rainfall is categorized as large according to the three-step strategy described in Section 2.1.2, meaning not all incoming runoff is required to infiltrate. Although diver data is unavailable to confirm this, it is expected that the detention basins were in use. As for Event 1, this is supported by the heightened water level in O1.

Event 3: February 10th, 2020

Event 3 started in the morning of February 12th and lasted until the subsequent evening. The total precipitation was 8.1 mm with an absolute peak of 2.4 mm between 10:00 and 11:00. The results are displayed in Table 7.3 and Figure 7.4. Air temperature remained above the freezing point for the duration of the rainfall but decreased gradually towards the end of the event.

Table 7.3: Results from Event 3.

	Volume [m ³]	Peak flow [l/s]	Time of peak
Precipitation	48.34		
Inflow	39.54	6.00	10.02.2020 10:38
Outflow	66.91	7.37	10.02.2020 10:42
Infiltration	12.61	0.92	10.02.2020 22:37

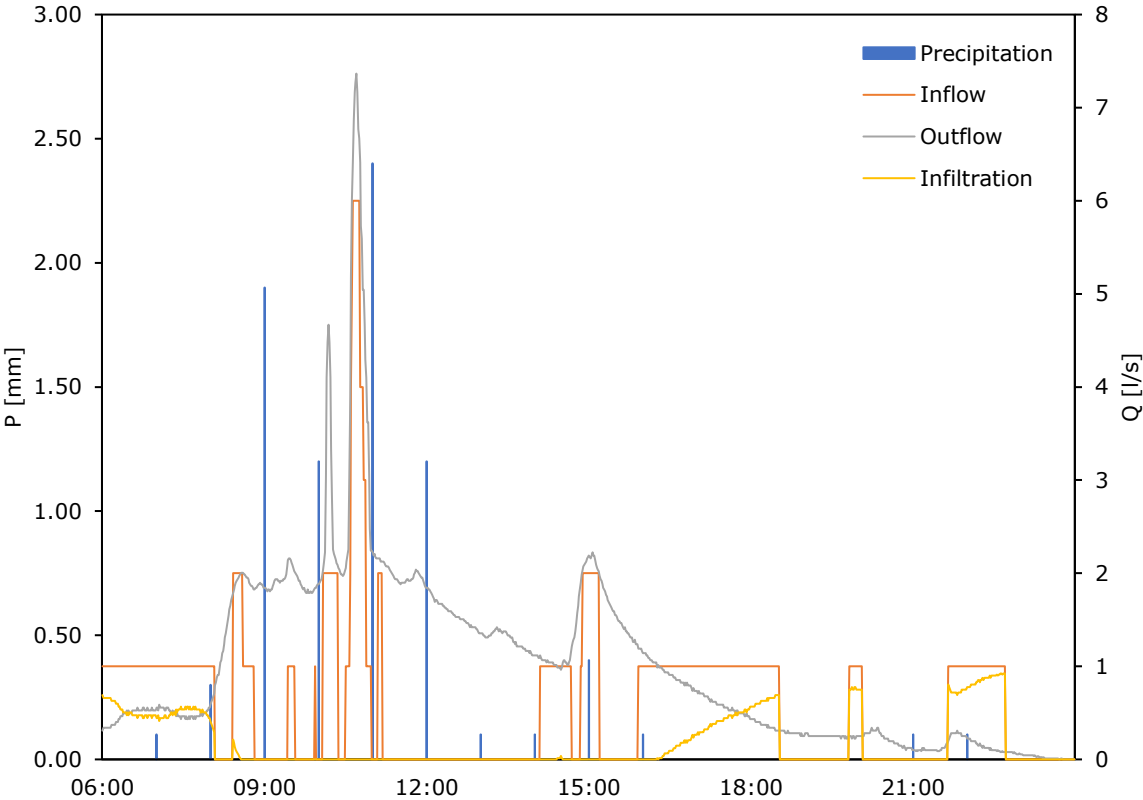


Figure 7.4: Results from Event 3.

Similar to Event 2, the inflow and outflow peaks occurred prior to the precipitation peak and is likely a result of local precipitation differences. However, the peaks in in- and outflow may also be a response to accumulated runoff from the preceding three hours. A few instances with 0.1 mm precipitation in an hour resulted in no apparent increase in inflow.

This implies that the runoff that reached the inlet, if any, was too small to be registered by the flow meter. Canopy interception and surface storage are two possible contributors to low inflow.

Like the two previous events, the outflow volume is higher than inflow, though to a smaller degree. The change in outflow follows a smoother pattern than inflow which makes the limitations of the inflow data processing, as discussed in Section 7.2.2, evident. Moreover, the gradual decrease in outflow following the inflow peaks implies that stormwater is being temporarily stored and the swirl chamber is limiting the flow onto the downstream piped network.

Infiltration appears to be falsely represented, as for Event 1. During the precipitation peak, infiltration is zero, which is unlikely. This would imply that K_{sat} was also equal to zero, or that clogging of the perforations in the infiltration pipes restricted infiltration entirely. In this case, infiltration appears to only be present when inflow is equal to 1.00 l/s. The combination of high outflow and an edged and uncertain inflow pattern appears to be resulting in the strange infiltration patterns.

Event 4: March 28th – 29th, 2020

Event 4 lasted from the evening of March 28th until the evening of March 29th, totalling 18.6 mm. The highest precipitation peak took place between 12:00 and 13:00 on March 29th, totalling 2.9 mm. The results are displayed in Table 7.4 and Figure 7.5. Air temperature was below freezing for most of the event. Starting at noon on March 29th, the temperature was above freezing for six consecutive hours.

Table 7.4: Results from Event 4.

	Volume [m³]	Peak flow [l/s]	Time of peak
Precipitation	112.38		
Inflow	76.38	2.00	29.03.2020 10:51
Outflow	40.53	1.46	29.03.2020 12:22
Infiltration	51.18	1.07	29.03.2020 10:51

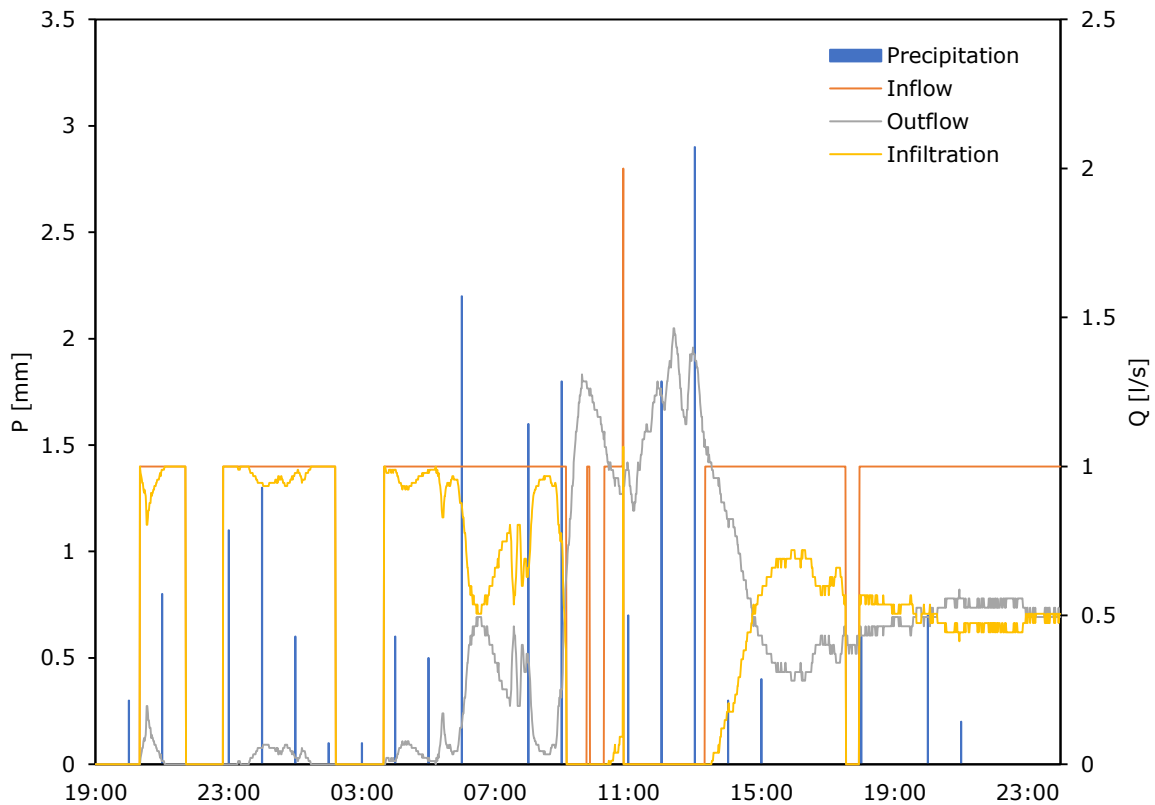


Figure 7.5: Results from Event 4.

This event is the first where inflow volume exceeds outflow, and where infiltration is relatively high. Inflow is 1.00 l/s for much of the rain event, but peaks at 2.00 l/s at 10:51 on March 29th. Outflow peaks 91 minutes later, at 1.46 l/s. As discussed previously, inflow and outflow may peak prior to precipitation due to local differences in rainfall.

During the first hours of the event, inflow and infiltration are practically equal. As precipitation increases, the amount of outflow starts to rise. Correspondingly, infiltration is decreased during this time. It is possible that the infiltration capacity of the perforated pipes was reached, or that the infiltration rate reached K_{sat} . Alternatively, the low air temperatures could have caused freezing rain in the early stages of the event; if so, it can be argued that the measured inflow during this time was false and caused from inaccuracies in data collection and processing. Water level in the detention basin farthest east, displayed in Appendix 10, shows no clear increase during this event, which also complies with high infiltration.

Event 5: April 15th, 2020

Event 5 took place on April 15th, starting in the morning and lasting until late evening. Precipitation was high for several consecutive hours, but an absolute peak of 2.8 mm occurred between 16:00 and 17:00. The total precipitation was 19.3 mm. The results are displayed in Table 7.5 and Figure 7.6. Air temperature was relatively low but remained above the freezing point for the duration of the event.

Table 7.5: Results from Event 5.

	Volume [m ³]	Peak flow [l/s]	Time of peak
Precipitation	116.61		
Inflow	43.80	8.00	15.04.2020 14:31
Outflow	61.85	6.14	15.04.2020 14:32
Infiltration	16.07	4.79	15.04.2020 17:01

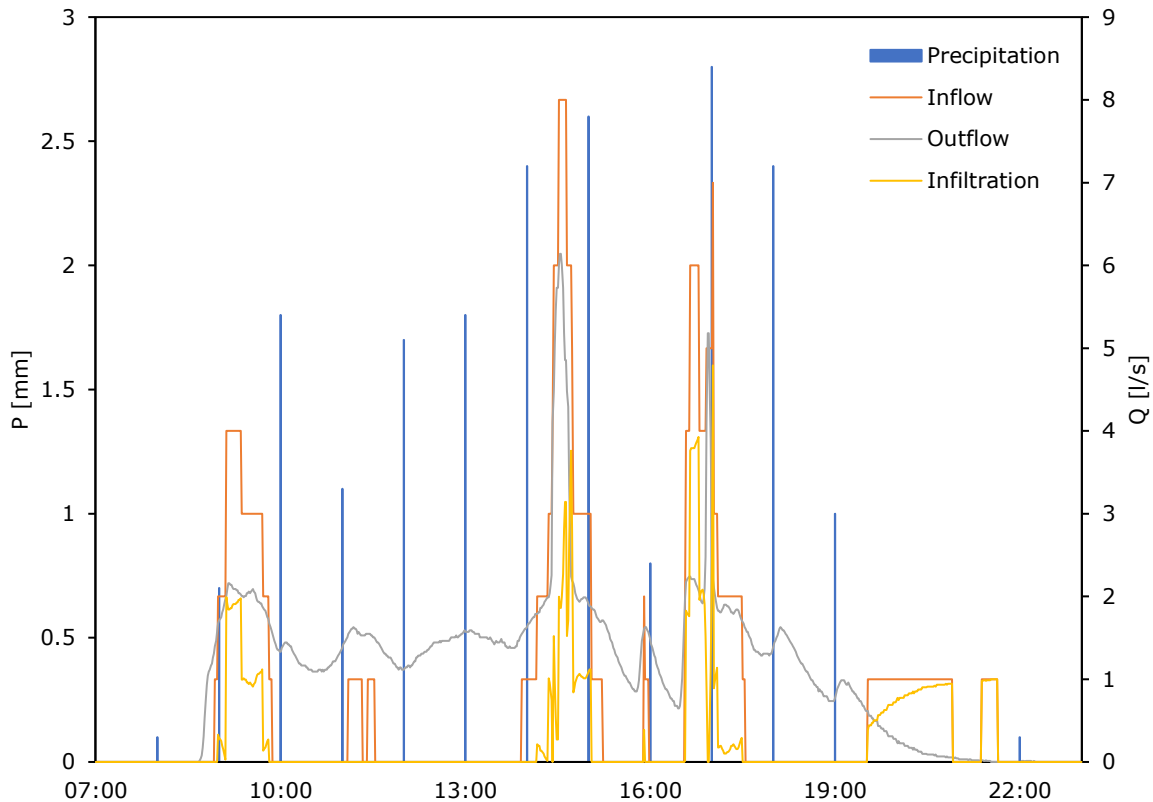


Figure 7.6: Results from Event 5.

Similar to Event 2 there are extended periods without inflow despite registered precipitation. Interception and surface storage may contribute to some extent, but local differences in precipitation is a more probable explanation with the current precipitation volumes.

Although outflow volume exceeds inflow, it should be pointed out that the inflow peaks at 9:11, 14:37 and 17:01 are higher than the corresponding outflow peaks. This explains the elevated infiltration during these times. From the figure in Appendix 10, an increase in detention basin water level can be seen during Event 5. This justifies the occasional high outflow and also implies that the maximum infiltration capacity was reached.

Event 6: May 6th, 2020

Event 6 took place on May 6th, totalling 10.8 mm. Three separate precipitation peaks of 2.2, 2.0 and 1.0 mm resulted in elevated in- and outflow. The highest precipitation peak occurred between 01:00 and 02:00. The results are displayed in Table 7.6 and Figure 7.7. Compared to the other events, air temperature was high during the event, ranging between 3.3 and 9.7 °C. This likely affected the response to the rainfall and may have resulted in a larger proportion of precipitation being lost to evaporation.

Table 7.6: Results from Event 6.

	Volume [m ³]	Peak flow [l/s]	Time of peak
Precipitation	65.25		
Inflow	40.62	14.00	06.05.2020 09:37
Outflow	10.39	6.77	06.05.2020 09:58
Infiltration	33.61	8.00	06.05.2020 09:59

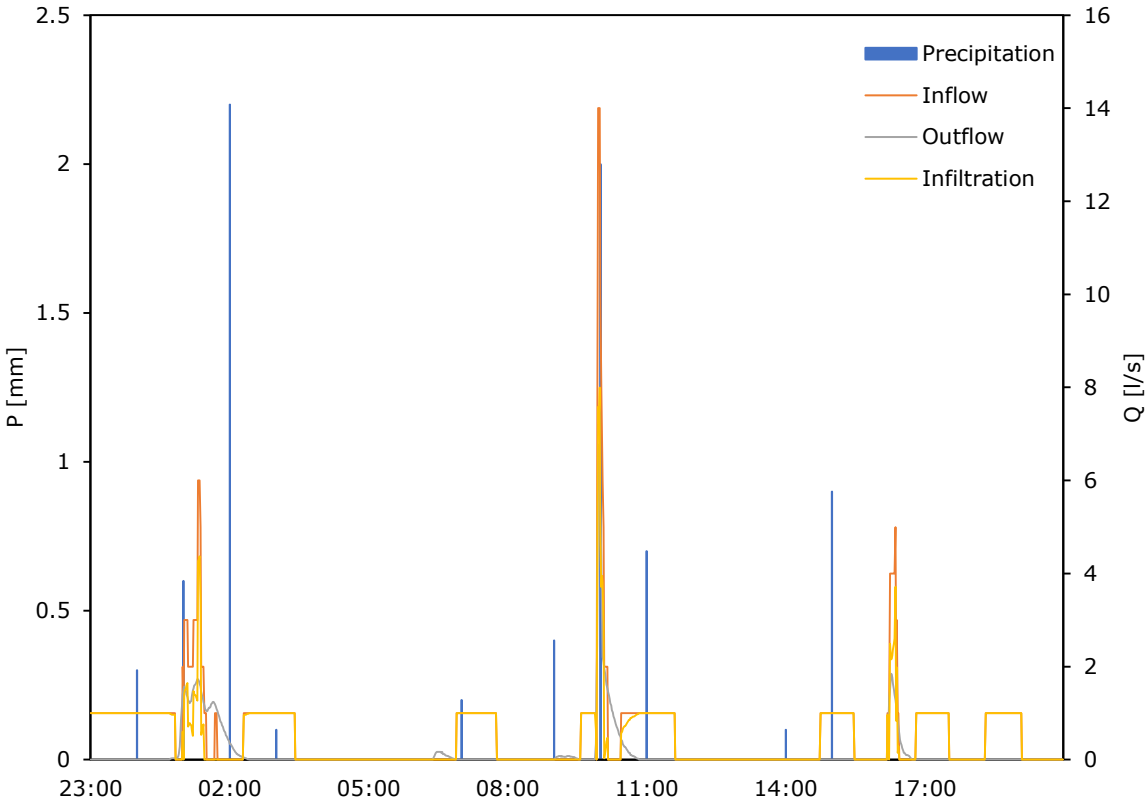


Figure 7.7: Results from Event 6.

Event 6 has low outflow compared to the other events and is significantly lower than both precipitation and inflow. In contrast to the other events, Event 6 is in accordance with the expected relationship between in- and outflow. The first in- and outflow highs occur prior to the first precipitation peak. As for Event 2, 3 and 4, this may be due to local differences in rainfall. It could be that the risen in- and outflow was a response to the prior precipitation, and that the 2.2 mm precipitation peak was limited to the area surrounding Risvollan.

Between 09:00 and 10:00, 2 mm of precipitation was measured. Interestingly, the response at the study site during this time is more apparent than for other similarly sized rainfalls. The inflow reaches a maximum of 14.00 l/s, while the maximum outflow was only 6.77 l/s. As a result, the infiltration was relatively high during this time. Again, local precipitation differences are probable contributing factors. Snow and sleet were observed during the event, and it can be argued that some precipitation was stored as snow at Risvollan, while at the study site it became runoff. Following the peak, inflow, outflow and infiltration gradually decrease to zero.

Following the last precipitation peak between 14:00 and 15:00, inflow and outflow increased before gradually declining and stabilising at zero. Generally, outflow decreases

at a slower rate than inflow which implies that runoff is temporarily stored within the facility. The two last elevations in inflow are most likely due to imperfections in the data processing.

7.4 Detention basin performance

As described in Section 5.1, the equipment for water level monitoring was installed in the detention basin farthest east. The complete graph showing the measured water level from March 10th to May 14th is shown in Appendix 10.

Data shows that there is approximately 1.5 cm of constant water table in the detention basin. Visual inspection also shows that even after extended dry periods the detention basin does not empty entirely, which likely is due to the basin design. Nonetheless, it appears that the detention basins are rarely in use, only for the largest registered rain events. Even then, the water level is low. For instance, the highest registered water level during Event 5 discussed above was 11.9 cm at 14:34, only few minutes after the in- and outflow peaks. The highest registered water depth during Event 6 was 14.6 cm at 11:00, approximately one hour after the inflow peak. This implies that the storage capacity may be unnecessarily large. Still, uncertainty with respect to large rain events is present. All registered rain events between March 10th and May 14th are categorized as small according to the three-step category. It is therefore expected that most of the incoming runoff is infiltrated, and the low degree of detention is reasonable. The data series is still short, and the basin performance during the larger February rains discussed previously remains uncertain.

7.5 Infiltration capacity evaluation

Due to the large uncertainty in available data, calculating infiltration capacity on site based on measured data is currently considered futile. Using information from previous core drillings and soil samples may at this stage be the best approach to estimating infiltration capacity, even though it may fail to consider the degrading effects of urbanization previously described. Properties of different soil types have been extensively studied in the past, and much knowledge on infiltration capacities exists. Infiltration rate during precipitation events ranges from 0 to 14.00 l/s based on Equation (13). Based on the collected data, there is no consistent response pattern to rainfall. It is unlikely that there is any major variation in infiltration performance between separate rain events, and it is assumed that the inconsistencies are mainly due to uncertainties in in- and outflow data.

The complete graph of calculated infiltration from February 1st to May 14th is shown in Appendix 9. The highest registered infiltration is 14.00 l/s and far less than the infiltration capacity estimated by Multiconsult (2018a), as described in Section 4.2.1. The soil infiltration capacity on site at this time is approximately 6.36×10^{-5} m/s, and the calculation based on Equation (12) is found in Appendix 11. This is within the range of values for hydraulic conductivity of sand but is somewhat smaller than what was initially assumed. Since infiltration for the most part is lower than 14.00 l/s it is possible that infiltration capacity is also lower, in accordance with the soil types found on site.

7.6 Possible system improvements

7.6.1 Inflow

As explained, inflow data was subject to noise and an incorrect threshold for zero flow. Data processing for noise removal was effective to some extent but resulted in rough inflow patterns not consistent with reality. For example, the inflow would sometimes increase instantly by 1 l/s without any apparent precipitation impacts, and soon thereafter drop back to zero. The flow meter was placed close to the inlet of manhole O8 which may have negatively impacted inflow data measurements. Some flow meters require a straight pipe segment of a certain length to obtain accurate measurements. With the absence of the continuous pipe through O17, the length of the straight pipe segment may be deficient. High-quality data may also be more difficult to obtain when the flow meter is exposed to turbulent flow near the inlet. The placement of the flow meter should therefore be evaluated with respect to external factors and disturbances.

7.6.2 Outflow

The current outflow data is highly uncertain due to the high uncertainty of the swirl chamber at low water levels. The outflow values included in Appendix 4 were determined experimentally, but no such data exists for water levels below the outlet centre line, as explained in Section 6.3.1. The outflow values for low water levels are therefore purely theoretical and have yet to be verified in practice.

Installing a flow meter downstream of the swirl chamber could improve the quality of outflow data. A venturi meter uses differential pressure to determine flow and is according to Aaby (2020) suitable for low pressure heads. However, the outlet pipe is continuous through manhole O16 which makes installation difficult. It is also recommended that the pressure sensor in O1 be calibrated regularly to improve data quality of water level measurements. This is especially important if a flow meter cannot be installed and outflow calculations based on pressure head are continued to be used. Though uncertainty in outflow calculations in themselves would be unchanged, the total uncertainty may be reduced with more certain water levels.

7.6.3 Precipitation

As explained in Section 5.1, installing a rain gauge on site was not possible due to the outbreak of Covid-19. The validity of the available precipitation data is therefore limited. Local weather differences are common, and for that reason installing a rain gauge closer to the study site should be a priority in future projects. This would improve validity and make data more suited for comparison with other measured data. A more thorough evaluation of the drainage area, as discussed in Section 7.2.1, is also recommended and may be useful in determining more accurate precipitation volumes.

7.6.4 Infiltration and detention

Water level on the upstream end of the facility is currently only measured in O17. These measurements can be used for comparison with inflow to O8 but say little about the detention basin usage. As illustrated in Figure 4.8, stormwater enters the detention basins when the water level in O8 exceeds 6.36 m.a.s.l. Installing a pressure cell in O8 for continuous monitoring of the water level could be useful and an alternative to divers inside the detention basin. Though the divers used in this study give valuable insight into the basin performance, a major disadvantage is that diver data must be collected on site with regular intervals of maximum 33 days with the current sample interval.

An alternative long-term solution for detention basin water level monitoring would also be desired. Decreasing the sample interval of the divers to five minutes would for example require data collection every 166 days. On the other hand, decreasing the sample interval may reduce certainty with respect to water level peaks. Preferably, a solution where water level data can be continuously collected is recommended. In addition, a web-camera and measurement scale installed inside the detention basin could be used in data collection if applying image analysis and also be used for verifying measured data from other equipment.

Several inaccurate input data to the infiltration calculations contribute to uncertain infiltration data. Implementing the above suggestions will likely improve the accuracy of infiltration estimates. Verifying the infiltration capacity estimated from measured data and soil properties is still recommended. Due to the impermeable surfaces, infiltration tests using ring infiltrometers is not possible on site. Performing such tests is still possible on permeable surfaces near the site. Although this would not give the exact infiltration capacity, it is assumed that soil properties in the Trondheim town centre are somewhat similar, and the result of an infiltration test may still be insightful.

Performing a controlled filling of the stormwater facility may also give valuable information about system performance. For example, by adding a known volume of water to the inlet at a predetermined rate, the hydraulic parameters can be continuously monitored and later analysed. A such process is not dependent on rainfall, and uncertainties related to drainage area and precipitation are eliminated.

8 Conclusion

The current study has evaluated the functionality and performance of a newly established system for sustainable urban stormwater management in Trondheim, Norway. The system combines infiltration and detention to safely divert stormwater runoff from the town square. The focus of this study has been on assessing the quality of the established monitoring system with respect to hydrological aspects and its usability for infiltration monitoring. The objective of this study was to answer the following thesis statement:

To what extent can infiltration capacity be estimated through continuous online monitoring of hydrological aspects accompanied with current knowledge on local soil conditions?

The thesis statement was supplemented with three research questions that will be answered in the following: (1) What are the strengths and weaknesses of the established system at Trondheim town square with respect to infiltration monitoring? (2) What improvements can be made to the system to increase the usability for infiltration monitoring? and (3) Preliminary analysis of system performance with respect to infiltration.

Strengths and weaknesses of the monitoring system

The established monitoring system at the stormwater facility provides some insight into the hydrological performance but fails to provide the necessary data for accurate infiltration results. The monitoring system setup is in theory suited for the purpose, but high uncertainty in several components of the data series is a major weakness. Inflow data is subject to noise and has an incorrect threshold for zero flow. Outflow must be calculated manually from water level measurements. Resulting data is highly uncertain for low outflow. Equipment for monitoring detention basin water levels was not included in the original system setup and was installed at a later stage. Subsequently, the data series are relatively short. Local differences in precipitation patterns have been apparent in the duration of the study and emphasize the importance of accurate weather data. The lack of precipitation measurements on site is therefore a significant limitation to the study.

Improvements to the monitoring system

Adjustments and modifications of the system setup may increase the usability with respect to infiltration monitoring. This applies mainly to inflow and outflow data quality. Ensuring the flow meter at the inlet is placed correctly and shielded from external disturbances may improve data quality. Installing a flow meter downstream of the swirl chamber would provide more tangible outflow data. Due to the current design of the SWM facility, installment of equipment on the downstream end may be intricate. Simpler adjustments, such as regular calibration of pressure cells, may therefore be most applicable for the time being. In addition, a permanent solution for water level measurements inside the detention basins would be advantageous for long term monitoring of detention basin performance. More accurate precipitation data can be obtained by installing a rain gauge near the study site, for example on the roof of a nearby building, and should be a priority before further research.

System performance

Preliminary analysis of the measurement data show that a portion of stormwater runoff entering the facility infiltrates to the subgrade soils. However, the estimated infiltration capacity is not as high as the local soil conditions imply and less than originally presumed. Infiltration varied greatly between events, depending on the inflow and outflow patterns. Regardless, the detention basins were seldomly used and appear to have a storage capacity sufficient even for extreme events and may be oversized for their purpose. The current study therefore concludes that infiltration capacity at the Trondheim town square cannot be stated with certainty from collected data, but to some extent be estimated when accompanied with current knowledge of local soil conditions.

8.1 Further work

Further research is needed to verify system performance with respect to infiltration and detention. Monitoring hydrological aspects after implementation of the above recommendations may be beneficial in more accurately determining infiltration capacity on site. Moreover, obtaining more accurate precipitation data should be prioritized in the future and will reduce uncertainty to a great extent. Performing a controlled filling of the facility allows for studying system performance while eliminating several sources of error related to precipitation and drainage.

In a longer perspective it may be interesting to study the long-term functionality of the system and the response to impacts commonly seen in urban areas. Clogging, maintenance, the effect of de-icing agents and climatic impacts are some factors that may influence the performance of the SWM system.

References

- Aaby, N. (2020) Outflow in swirl chamber, 5. April.
- Aas, M. I. and Muthanna, T. M. (2017) Infiltrasjonssandfang - Dimensjoneringskriterier og kapasitetsmåling: NTNU.
- Al-Rubaei, A. M. *et al.* (2013) Long-Term Hydraulic Performance of Porous Asphalt Pavements in Northern Sweden, *Journal of Irrigation and Drainage Engineering*, 139(6), pp. 499-505. doi: 10.1061/(ASCE)IR.1943-4774.0000569.
- Autodesk (2020) AutoCAD (23.1.47.0 edn.).
- Ballard, B. W. *et al.* (2015) *The SuDS Manual*. London, UK: CIRIA.
- Balstad, S. *et al.* (2018) Seasonal variations in infiltration in cold climate raingardens - a case study from Norway, *VANN*, 53(1), pp. 5-14.
- Basal AS (n.d.) *BASAL Qmax-V*. Available at: <https://www.basal.no/produkt/17/qmax-v> (Accessed: 15. April 2020).
- Bonneau, J. *et al.* (2017) Stormwater infiltration and the 'urban karst' – A review, *Journal of Hydrology*, 552, pp. 141-150. doi: 10.1016/j.jhydrol.2017.06.043.
- Brattli, B. (2009) *Fysisk og kjemisk hydrogeologi*. 3. utg. edn. Trondheim: NTNU, Institutt for geologi og bergteknikk.
- Butler, D. and Davies, J. W. (2011) *Urban Drainage*. 3rd edn. Abingdon, Oxon: Spon Press.
- Campbell Scientific (2020) *CR310*. Available at: <https://www.campbellsci.com/cr310> (Accessed: 4. March 2020).
- COWI (2015) *Gjennomgang av avrenningsfaktorer*. Available at: <http://www.miljodirektoratet.no/Documents/publikasjoner/M293/M293.pdf> (Accessed: 26. april 2018).
- Darcy, H. P. G. (1856) *Les Fontaines publiques de la ville de Dijon. Exposition et application des principes à suivre et des formules à employer dans les questions de distribution d'eau, etc.* V. Dalamont.
- Dingman, S. L. (2015) *Physical hydrology*. 3 edn. Long Grove, Illinois: Waveland press.
- Eckart, K., McPhee, Z. and Bolisetti, T. (2017) Performance and implementation of low impact development - A review, *Science of the Total Environment*, 2017(607-608), pp. 413-432. doi: 10.1016/j.scitotenv.2017.06.254.
- Emdal, A. (2020) Rotary pressure sounding, 14. February.
- Endresen, S. and Sweco (2019) *Infiltrasjon av overvann*. (92): VA/Miljø-blad. Available at: <https://www.va-blad.no/overflateinfiltrasjon/> (Accessed: 14. October 2019).
- Fletcher, T. D., Andrieu, H. and Hamel, P. (2013) Understanding, management and modelling of urban hydrology and its consequences for receiving waters: A state of the art, *Advances in Water Resources*, 51(2013), pp. 261-279. doi: 10.1016/j.advwatres.2012.09.001.
- Gregory, J. *et al.* (2006) Effect of urban soil compaction on infiltration rate, *Journal of Soil and Water Conservation*, 61(3), pp. 117-124.
- Holm, E. (2013) *Regnbed, renner og nedslivningsarealer*. (106): VA/Miljø-blad. Available at: <https://www.va-blad.no/regnbed-renner-og-nedslivningsarealer/> (Accessed: 31. January 2020).
- Horton, R. E. (1941) An approach toward a physical interpretation of infiltration-capacity 1, *Soil science society of America journal*, 5(C), pp. 399-417.
- Huang, J. *et al.* (2016) Three Types of Permeable Pavements in Cold Climates: Hydraulic and Environmental Performance, *Journal of Environmental Engineering*, 142(6). doi: 10.1061/(ASCE)EE.1943-7870.0001085.
- Johannessen, B. and Muthanna, T. (2018) Detention and Retention Behavior of Four Extensive Green Roofs in Three Nordic Climate Zones, *Water*, 10(6), pp. 671. doi: 10.3390/w10060671.

- Johannessen, B. G., Hanslin, H. M. and Muthanna, T. M. (2017) Green roof performance potential in cold and wet regions, *Ecological Engineering*, 106(PA), pp. 436-447. doi: 10.1016/j.ecoleng.2017.06.011.
- Kartverket (2020a) *Basemap: Air photo*. Available at: https://www.norgeskart.no/?test=1&_ga=2.126625028.808749792.1579770071-62749183.1578565355#!?project=seeiendom&layers=1003&zoom=13&lat=7041666.16&lon=270335.90.
- Kartverket (2020b) *Basemap: Grayscale*. Available at: https://www.norgeskart.no/?test=1&_ga=2.126625028.808749792.1579770071-62749183.1578565355#!?project=seeiendom&layers=1005&zoom=3&lat=7149040.58&lon=356963.88.
- Kaushal, S. and Belt, K. (2012) The urban watershed continuum: evolving spatial and temporal dimensions, *Urban Ecosystems*, 15(2), pp. 409-435. doi: 10.1007/s11252-012-0226-7.
- Lindholm, O. et al. (2008) *Veiledning i klimatilpasset overvannshåndtering*. (162 - 2008): Norsk Vann.
- Lindholm, O. et al. (2012) *Veiledning i dimensjonering og utforming av VA-transportsystem*. (193 - 2012): Norsk Vann.
- Lindholm, O. (2018) *Håndtering av overvann : LOD*. (125): VA/Miljø-blad. Available at: <https://www.va-blad.no/handtering-av-overvann-lod/> (Accessed: 31. January 2020).
- Magnussen, K. et al. (2015) *Kostnader og nytte ved overvannstiltak, Oslo: Vista Analyse AS*.
- Meteorologisk institutt (2017) *Trøndelag siden 1900*. Available at: <https://www.met.no/vaer-og-klima/klima-siste-150-ar/regionale-kurver/trondelag-siden-1900> (Accessed: 07. January 2020).
- MFT (2018) *Teknisk beskrivelse og dokumentasjon*. (Trondheim. Oppgradering torget.).
- MFT (2020) *FluidVertic VSU*. Available at: <https://mft.no/mengderegulatorer/fluidvertic-vs/#funksjon> (Accessed: 2020 8. April).
- Minasny, B. and McBratney, A. B. (2003) Integral energy as a measure of soil-water availability, *Plant and Soil*, 249(2), pp. 253-262. doi: 10.1023/A:1022825732324.
- Monrabal-Martinez, C. et al. (2019) Infiltration Response of Adsorbent Amended Filters for Stormwater Management under Freezing/Thawing Conditions, *Water*, 11(12). doi: <https://doi.org/10.3390/w11122619>.
- Multiconsult (2017) *Fordrøyning av overflatevann fra torgflata*. (Torvet i Trondheim 417316-4-RIVA-NOT-001).
- Multiconsult (2018a) *Infiltrasjon av overflatevann fra torgflata*. (Torvet i Trondheim 417316-04-RIVA-NOT-002).
- Multiconsult (2018b) *Geotekniske grunnundersøkelser*. (Torvet i Trondheim - Byrom og parkeringsanlegg 417316-RIG-RAP-001).
- NGU (2019) *Nasjonal løsmassedatabase*. Available at: <http://geo.ngu.no/kart/losmase/> (Accessed: 9. January 2020).
- Norsk Klimaservicesenter (2016) *Klimaprofil Sør-Trøndelag : Et kunnskapsgrunnlag for klimatilpassning*. Norsk Klimaservicesenter.
- Norsk Klimaservicesenter (2020) *Observasjoner og værstatistikk*. Available at: <https://seklima.met.no/observasjoner> (Accessed: 13. March 2020).
- Paus, K. H., Muthanna, T. M. and Braskerud, B. C. (2016) The hydrological performance of bioretention cells in regions with cold climates: seasonal variation and implications for design, *Hydrology Research*, 47(2), pp. 291-304. doi: 10.2166/nh.2015.084.
- Pitt, R. et al. (1999) *Infiltration Through Disturbed Urban Soils and Compost-Amended Soil Effects on Runoff Quality and Quantity*. (EPA/600/R-00/016 (NTIS PB2000-102012)). Washington, DC: U.S. Environmental Protection Agency. Available at: <http://nepis.epa.gov/Exe/ZyPURL.cgi?Dockey=P1000OBH.txt>.
- Pitt, R., Chen, S.-E. and Clark, S. (2002) Compacted Urban Soils Effects on Infiltration and Bioretention Stormwater Control Designs, *Global Solutions for Urban Drainage, Portland, OR, United States*. pp. 1-21.

- Prince George's County (1999) *Low-Impact Development Hydrologic Analysis*. Available at: https://engineering.purdue.edu/mapserve/LTHIA7/documentation/downloads/LID_HYDR.PDF.
- Rosen, R. M. *et al.* (2012) Water Quality and Hydrologic Performance of a Porous Asphalt Pavement as a Storm-Water Treatment Strategy in a Cold Climate, *Journal of Environmental Engineering*, 138(1), pp. 81-89. doi: 10.1061/(ASCE)EE.1943-7870.0000459.
- Sage, J., Berthier, E. and Gromaire, M.-C. (2015) Stormwater management criteria for on-site pollution control: a comparative assessment of international practices, *Environmental management*, 56(1), pp. 66-80. doi: <https://doi.org/10.1007/s00267-015-0485-1>.
- Seametrics (n.d.) *PT12*. Available at: <https://www.seametrics.com/wp-content/uploads/LT14338r25-20180306-PT12-Specs.pdf> (Accessed: 4. March 2020).
- Sharp, J. M. and Garcia-Fresca, B. (2003) Effects of urbanization on groundwater resources, recharge rates, and flow patterns (vol. 35, pp. 257-278). Boulder, Colorado: Geological Society of America (GSA).
- Skaaraas, H. *et al.* (2015) *Overvann i byer og tettsteder - Som problem og ressurs*. (NOU 2015 16). Oslo. Available at: <https://www.regjeringen.no/no/dokumenter/nou-2015-16/id2465332/> (Accessed: 16. December 2019).
- Statistisk sentralbyrå (2020a) *Kommunefakta - Bergen*. Available at: <https://www.ssb.no/kommunefakta/bergen> (Accessed: 14. January 2020).
- Statistisk sentralbyrå (2020b) *Kommunefakta - Oslo*. Available at: <https://www.ssb.no/kommunefakta/oslo> (Accessed: 14. January 2020).
- Statistisk sentralbyrå (2020c) *Kommunefakta - Trondheim*. Available at: <https://www.ssb.no/kommunefakta/trondheim> (Accessed: 14. January 2020).
- Trondheim kommune (1970) *Kongens gate - Grunnboringsrapport*. (0200).
- Trondheim kommune (2001) *Trondheim Torg - Grunnundersøkelser datarapport*. (1129).
- Trondheim kommune (2013) *Hovedplan avløp og vannmiljø 2013-2024*.
- Trondheim kommune (2015) *Beregning av overvannsmengde - Dimensjonering av ledning og fordrypningsvolum*. Available at: <http://132522-www.web.tornado-node.net/wp-content/uploads/2016/05/Vedlegg-5-Beregning-av-overvannsmengde.pdf> (Accessed: 15. January 2020).
- Trondheim kommune (2019) *Torvet, grunnvannsstandsmåling*. (1751).
- United Nations, D. o. E. a. S. A., Population Division, (2019a) *World Urbanization Prospects: The 2018 Revision*. (ST/ESA/SER.A/420). New York: United Nations. Available at: <https://population.un.org/wup/Publications/Files/WUP2018-Report.pdf>.
- United Nations, D. o. E. a. S. A., Population Division, (2019b) *World population prospects : 2019 : highlights*. (ST/ESA/SER.A/423). New York: United Nations. Available at: https://population.un.org/wpp/Publications/Files/WPP2019_Highlights.pdf.
- University of Arkansas Community Design Center (2010) *Low Impact Development: a design manual for urban areas*. Fayetteville, Arkansas: University of Arkansas Press.
- Van Essen Instruments (2016) *Diver Product Manual*. Available at: <https://www.vanessen.com/images/PDFs/Diver-ProductManual-en.pdf> (Accessed: 16. March 2020).
- Van Essen Instruments (2019) *Diver-Office* (11.0.0.1 edn.).
- Van Genuchten, M. T. (1980) A closed-form equation for predicting the hydraulic conductivity of unsaturated soils 1, *Soil science society of America journal*, 44(5), pp. 892-898. doi: 10.2136/sssaj1980.03615995004400050002x.
- Vatankhah, A. R. (2016) Discussion of "Stage-Discharge Models for Concrete Orifices: Impact on Estimating Detention Basin Drawdown Time" by WT Barlow and D. Brandes, *Journal of Irrigation and Drainage Engineering*, 142(11).
- Viatronics (n.d.) *Pipeline AVSS*. Available at: <http://www.viatronics.fi/uploads/Brochures/Viatronics-Pipeline-SVR-AVSS.pdf> (Accessed: 4. March 2020).

- Vista Engineering (2019) *Vista Data Vision*. Available at: <http://graf.itasdata.no/index.html> (Accessed: 7. February 2020).
- Water Environment Federation and ASCE (2012) *Design of urban stormwater controls*. 2 edn. New York: McGraw-Hill Professional.
- Yang, J.-L. and Zhang, G.-L. (2011) Water infiltration in urban soils and its effects on the quantity and quality of runoff, *Journal of Soils and Sediments*, 11(5), pp. 751-761. doi: 10.1007/s11368-011-0356-1.
- Ødegaard, H. *et al.* (2014) *Vann- og avløpsteknikk*. 2 edn. Hamar: Norsk Vann.

Appendices

Appendix 1: Planar view of Trondheim town square

Appendix 2: Detailed view of infiltration facility

Appendix 3: Noise removal code

Appendix 4: Calculated data for hydraulic characteristics of swirl chamber

Appendix 5: Precipitation data from Risvollan

Appendix 6: Air temperature data from Risvollan

Appendix 7: Inflow data

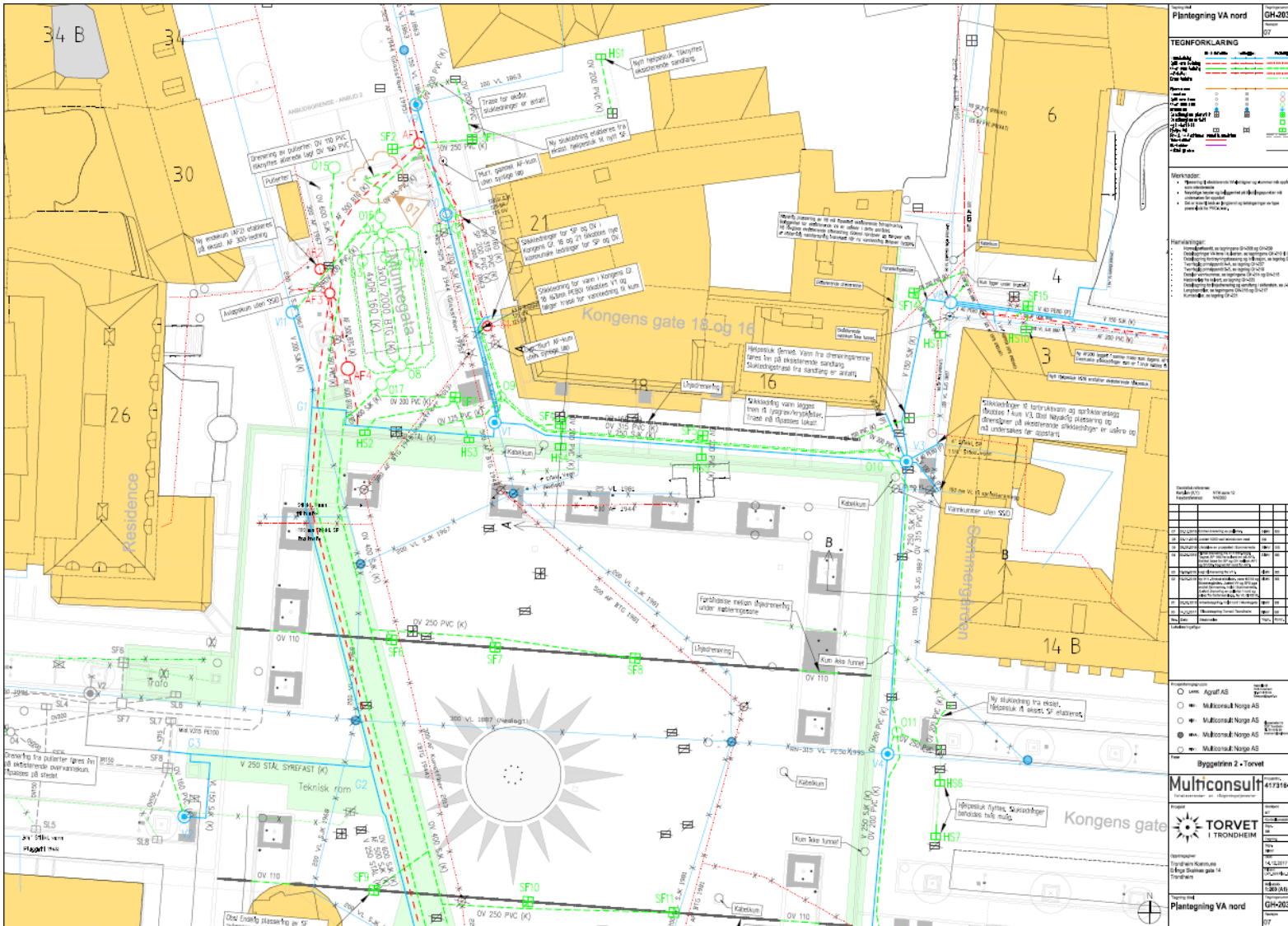
Appendix 8: Outflow data

Appendix 9: Calculated infiltration

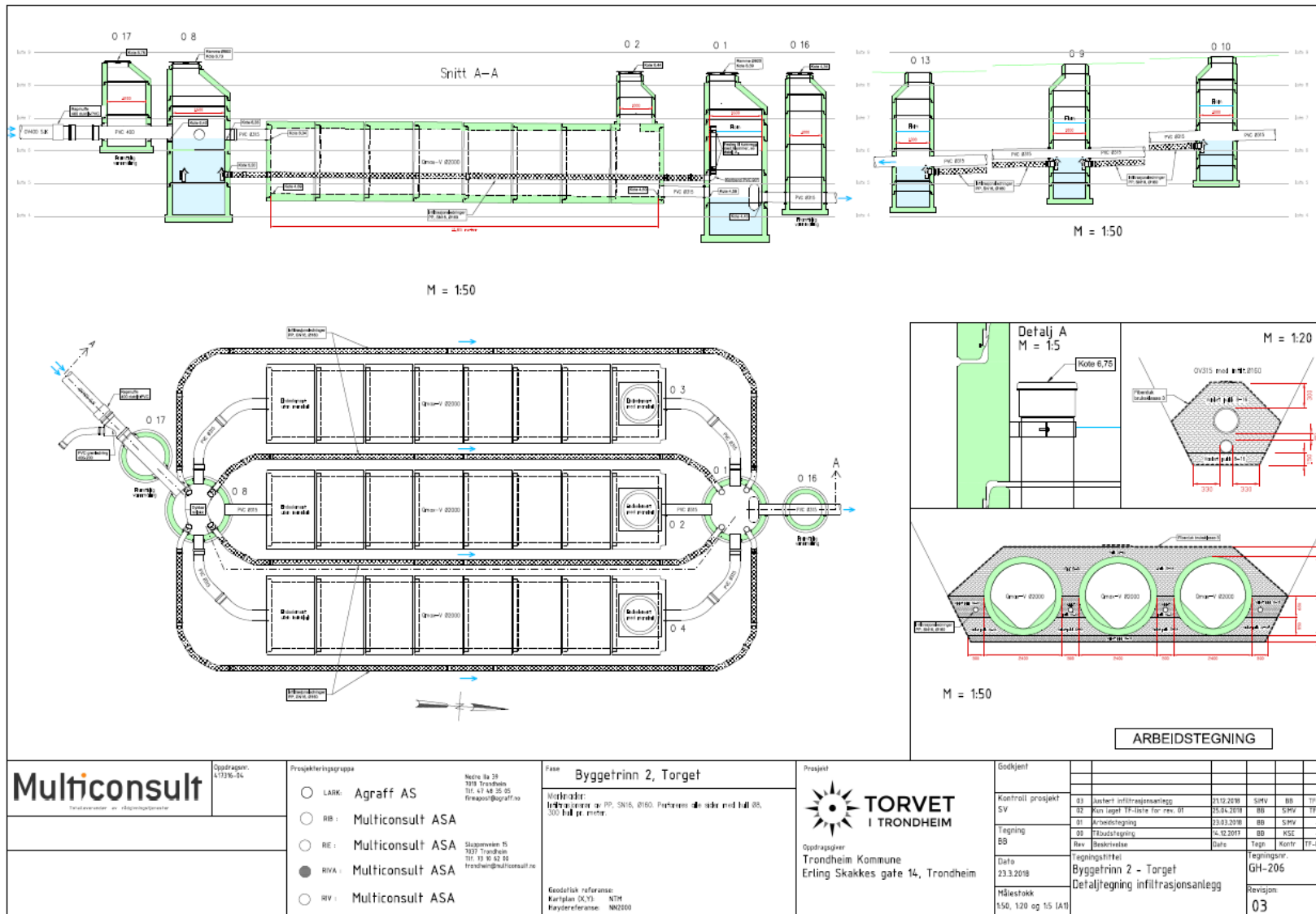
Appendix 10: Water depth in detention basin

Appendix 11: Calculation of soil infiltration capacity

Appendix 1: Planar view of Trondheim town square



Appendix 2: Detailed view of infiltration facility



Multiconsult
Ingeniør- og rådgivningsfirma

Oppdragsnr.:
L1336-56

Prosjektforingsgruppe

- LARK: Agraff AS
- RB: Multiconsult ASA
- RE: Multiconsult ASA
- RIVA: Multiconsult ASA
- RV: Multiconsult ASA

Agroff AS
Nedre Ila 28
7018 Trondheim
Tlf: 47 48 35 05
firmag@agraff.no

Sjøstovveien 15
3337 Trondheim
Tlf: 91 95 92 58
trondwin@multiconsult.no

Fase: Byggetrinn 2, Torget

Utvikler:
Hydroingeniør as, PP, SN15, Ø160. Parkerer alle biler med full ØS,
500 full pr. område.

Geoteknisk referanse:
Kartplan 02.73 NTH
Fagreferanse: NN2100

Prosjekt



Oppdragsveier:
Trondheim Kommune
Erling Skakkes gate 14, Trondheim

Godkjent

Kontroll prosjekt	SV	Dato	SHV	BB	TF-L5
03	Instert infiltrasjonsanlegg	21.12.2018	SHV	BB	TF-L5
02	Kon liget TF-liste for rev. 01	05.04.2018	BB	SHV	TF-L5
01	Arbeidstegning	23.03.2018	BB	SHV	-
09	Flussdiagram	16.12.2017	BB	KSE	-
Rev	Beskrivelse	Dato	Tegn	Kontr	TF-liste
Tegningsstiftet			Tegningsnr.		
Byggetrinn 2 - Torget			GH-206		
Detaljtegning infiltrasjonsanlegg			Revisjon		
Målestokk			03		
1:50, 1:20 og 1:5 (A1)					

Appendix 3: Noise removal code

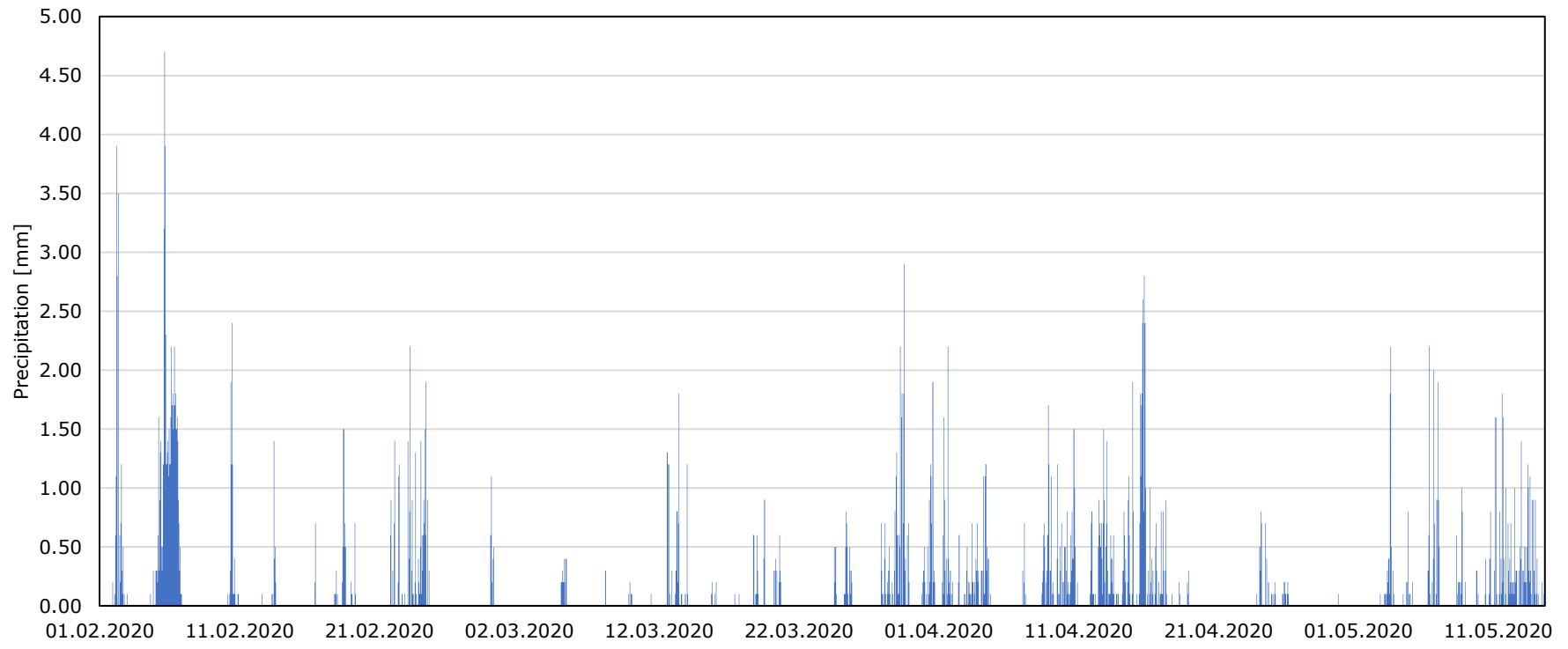
```
# import data #
data.file.link = "C://Users//Pernille//OneDrive - NTNU//Master//R//Data.csv"
data1 = read.table(data.file.link,header = TRUE, sep = ";")
inflow_1min= data1$X1810_Tr_Torg_min..Pipe_flow.m3.s.
old_inflow = data1$X1810_Tr_Torg_min..Pipe_flow.m3.s.
n = nrow(data1)

# code for noise removal #
k = 1
for(i in 1:n) {
  for(j in 2:5) {
    if (inflow_1min[i] == inflow_1min[i+j]) {
      if(inflow_1min[i+1] != inflow_1min[i]) {
        for (y in 1:k){
          inflow_1min[i+y] = inflow_1min[i]
        }
      }
    }
    k = k + 1
  }
  k = 1
}
```

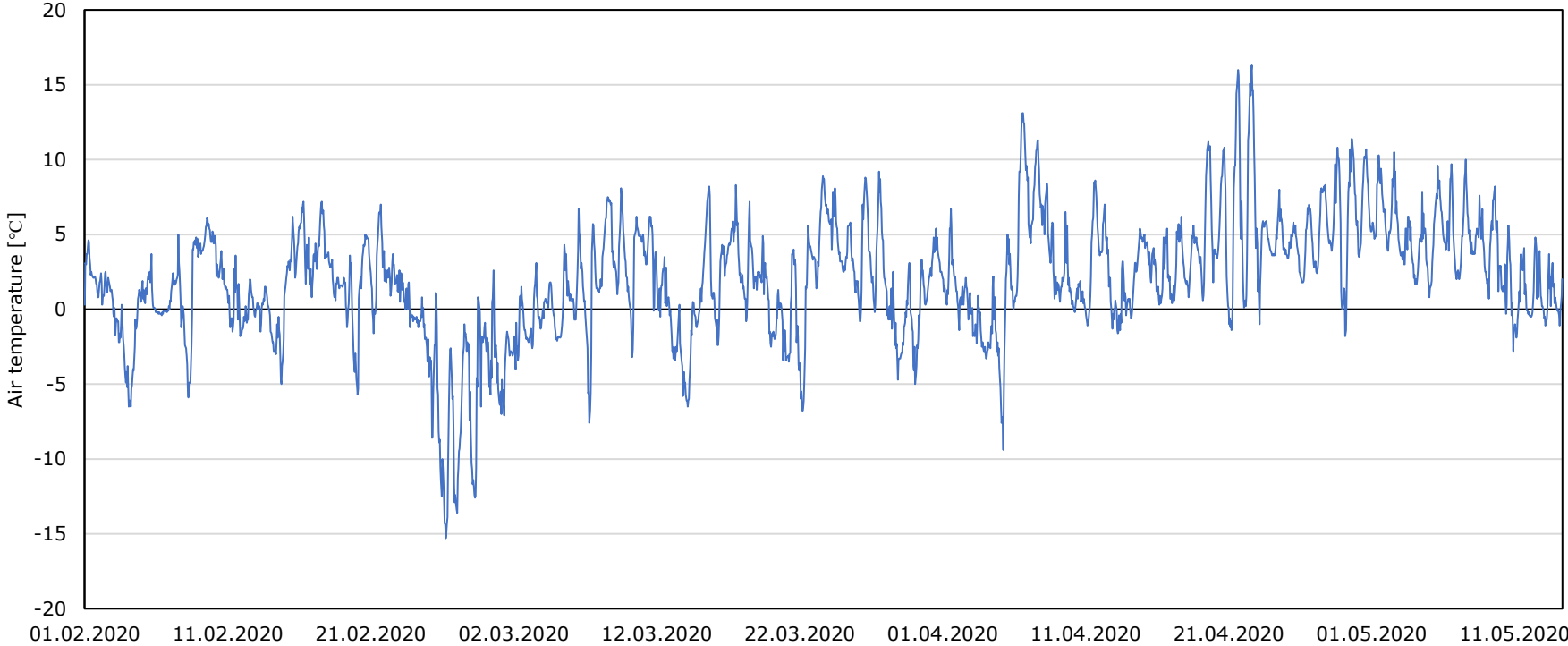
Appendix 4: Calculated data for hydraulic characteristics of swirl chamber

h_r (m)	Q_{out} (l/s)	h_r (m)	Q_{out} (l/s)	h_r (m)	Q_{out} (l/s)
0.003	2.26	0.225	13.16	0.600	14.24
0.009	3.93	0.244	13.25	0.675	14.91
0.015	5.04	0.263	13.34	0.750	15.63
0.027	6.63	0.281	13.35	0.938	17.36
0.037	7.71	0.300	13.33	1.125	18.96
0.056	9.13	0.319	13.33	1.312	20.43
0.075	10.26	0.338	13.35	1.500	21.79
0.094	11.13	0.356	13.35	2.300	26.72
0.113	11.76	0.375	13.34	3.188	31.16
0.131	12.20	0.412	13.33	4.687	37.33
0.150	12.53	0.450	13.36	6.562	43.76
0.169	12.82	0.487	13.48	7.500	46.62
0.188	13.05	0.525	13.69		
0.206	13.12	0.562	13.95		

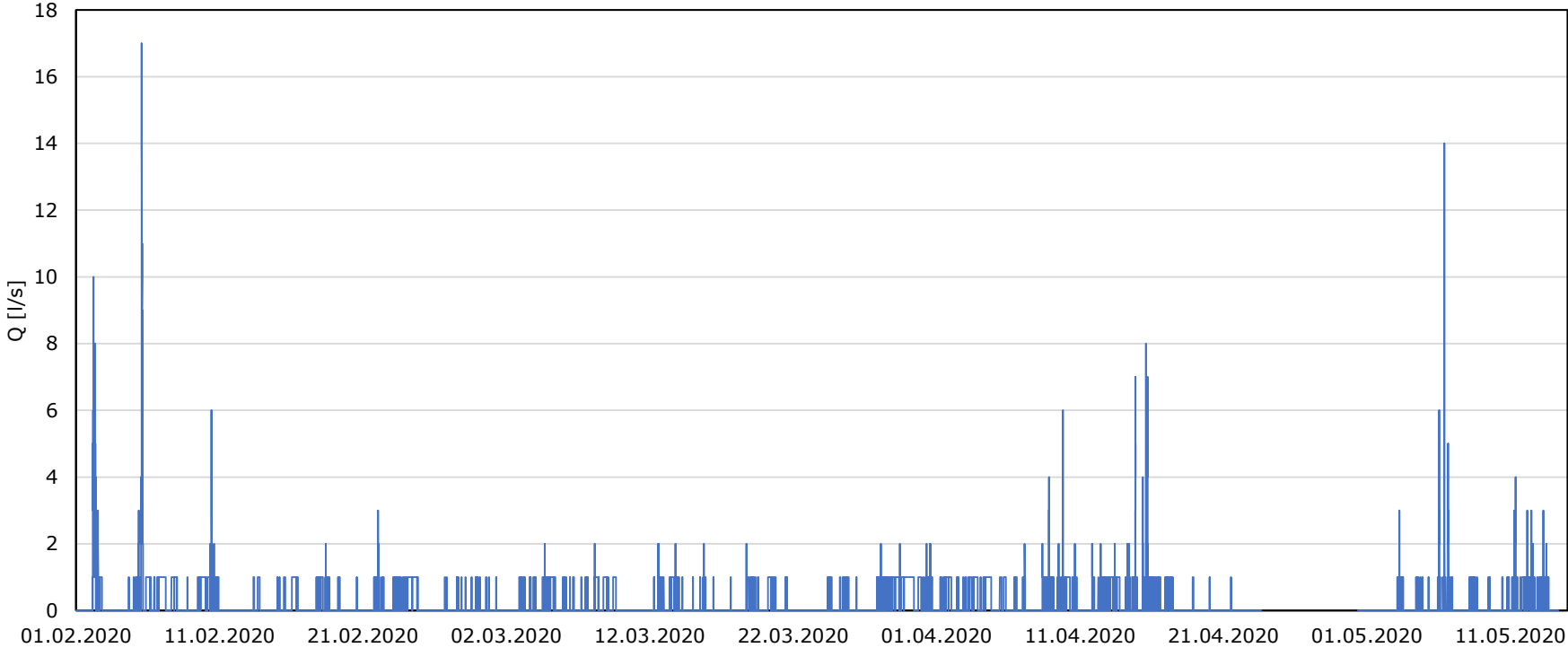
Appendix 5: Precipitation data from Risvollan



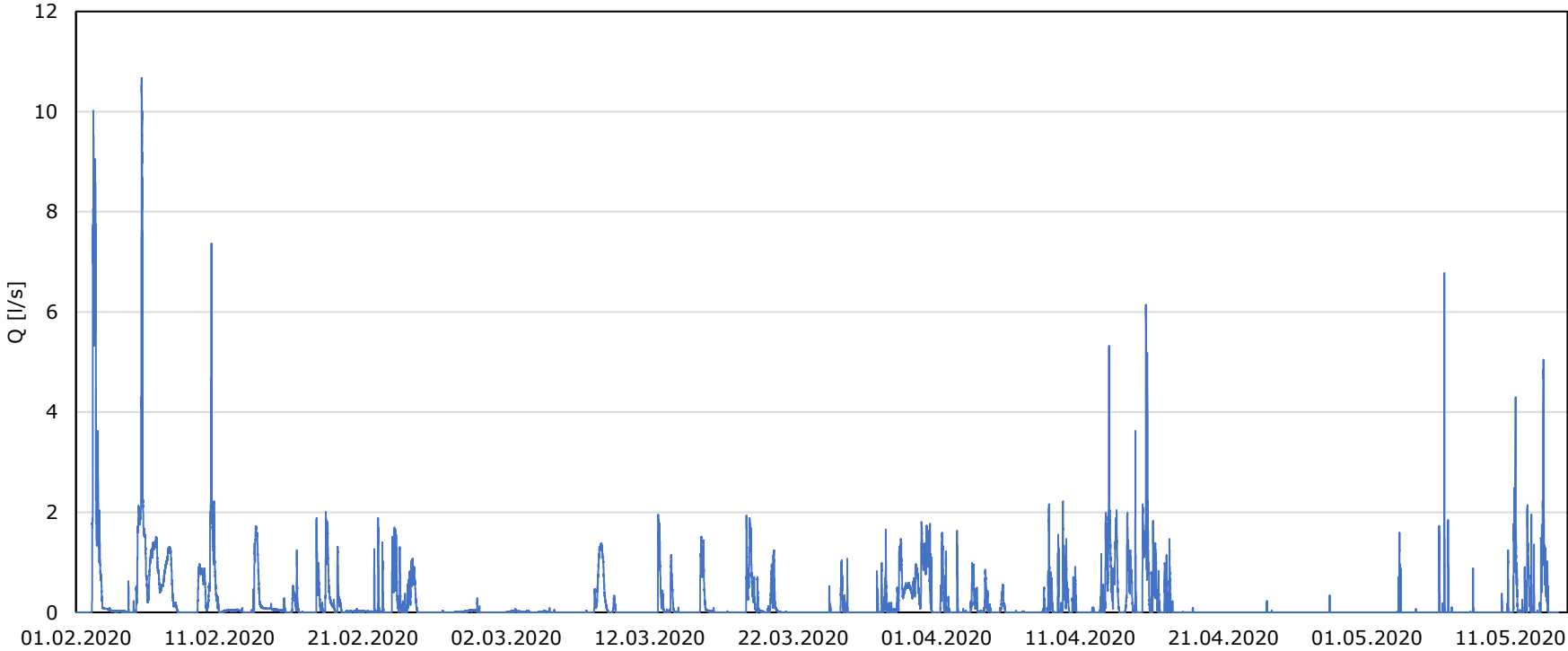
Appendix 6: Air temperature data from Risvollan



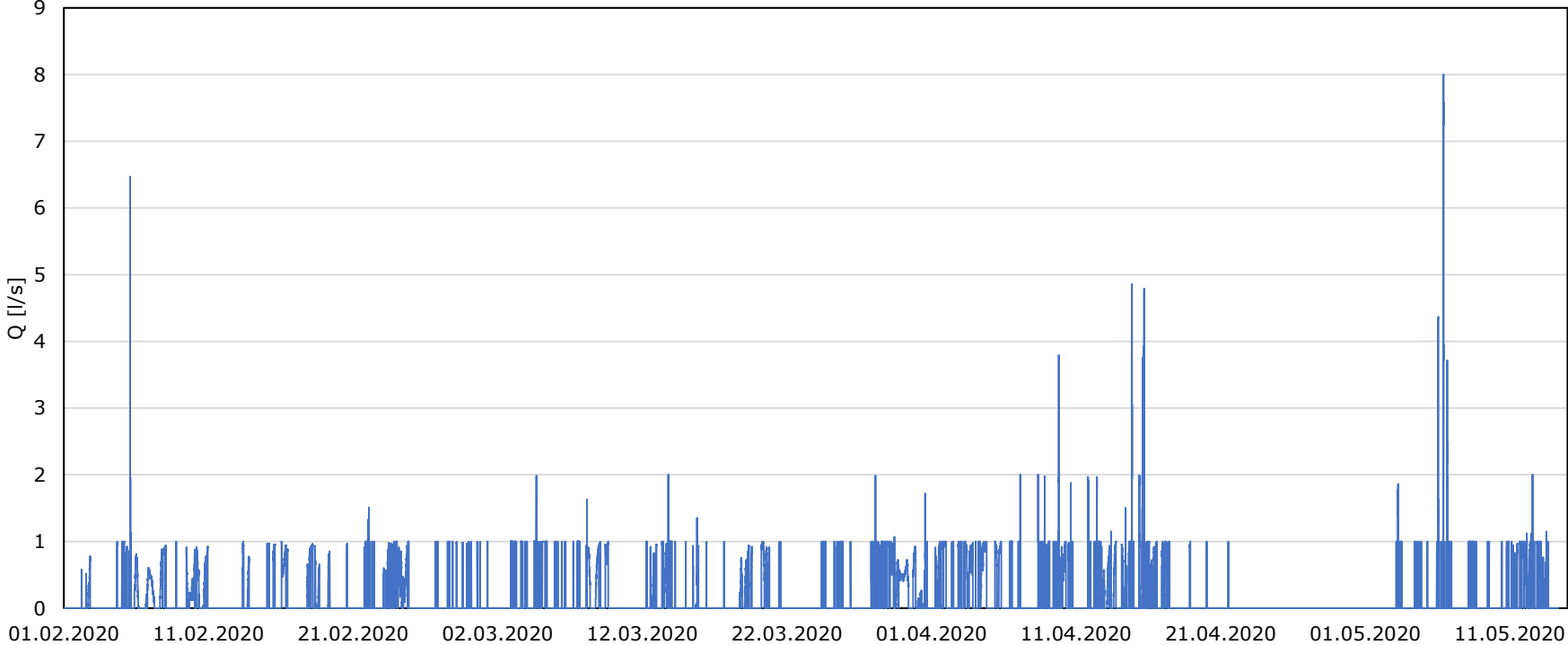
Appendix 7: Inflow data



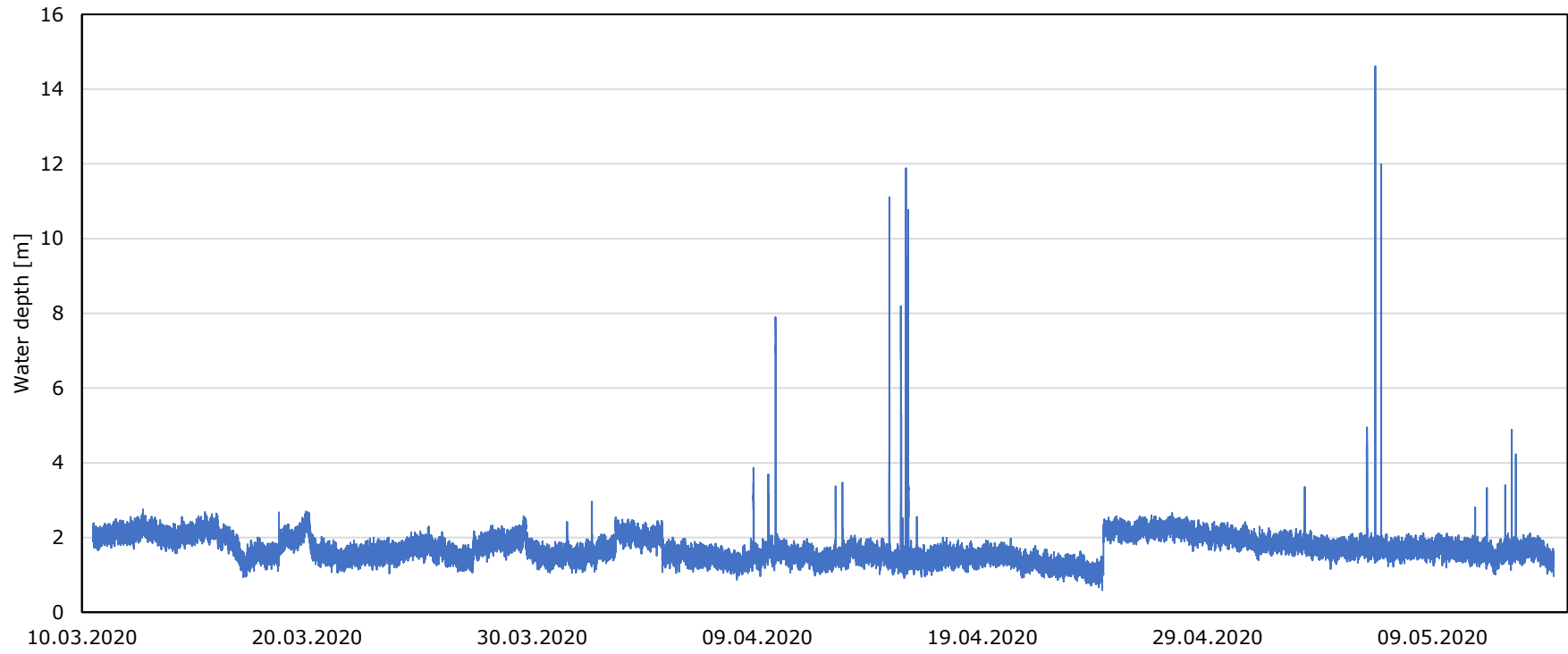
Appendix 8: Outflow data



Appendix 9: Calculated infiltration



Appendix 10: Water depth in detention basin



Appendix 11: Calculation of soil infiltration capacity

Length of infiltration area

$$\begin{aligned}l &= \frac{q_{inf}}{k \cdot w} \\ &= \frac{220 \cdot 10^{-3} \text{ m}^3/\text{s}}{0.001 \text{ m/s} \cdot 23 \text{ m}} \\ &= 9.57 \text{ m}\end{aligned}$$

Hydraulic conductivity

$$\begin{aligned}k &= \frac{Q_{inf}}{l \cdot w} \\ &= \frac{14.00 \cdot 10^{-3} \text{ m}^3/\text{s}}{9.57 \text{ m} \cdot 23 \text{ m}} \\ &= 6.36 \cdot 10^{-5} \text{ m/s}\end{aligned}$$

